

DESCRIPTION OF THE LOCAL LEVEL INERTIAL SURVEY SYSTEM AND ITS SIMULATION

JOHN R. ADAMS

April 1979



TECHNICAL REPORT
NO. 59

PREFACE

In order to make our extensive series of technical reports more readily available, we have scanned the old master copies and produced electronic versions in Portable Document Format. The quality of the images varies depending on the quality of the originals. The images have been converted to searchable text.

DESCRIPTION OF THE LOCAL LEVEL INERTIAL
SURVEY SYSTEM AND ITS SIMULATION

by

John R. Adams

Department of Surveying Engineering
University of New Brunswick
Fredericton, N.B.

April, 1979

PREFACE

This report is an unaltered version of the author's masters thesis entitled "Local Level Inertial Survey System".

The thesis advisors under whom this work was carried out were Dr. D. B. Thomson and Dr. K. P. Schwarz. Acknowledgement of the assistance rendered by others is given in the Acknowledgements.

ABSTRACT

Inertial survey systems are complex electro-mechanical devices from which one may determine position, velocity, acceleration, and gravity information. This complexity demands a complete and clearly outlined description of the inertial device itself and the environment within which it must operate. The first part of this thesis concerns itself with these topics, with special attention paid to the Local Level inertial survey system currently used in the surveying industry. The high accuracies required in surveying applications and the special updating procedures needed to attain them make it necessary to provide the rigorous mathematical derivation of the mechanization equations presented in this thesis.

The complexity and interaction of the various components make it very difficult to properly analyze the inertial system response to different error sources in a purely analytical way. Previous attempts have relied on numerous approximations for solving the analysis problem. To eliminate these difficulties a computer simulation program of approximately 1 800 FORTRAN statements has been written and was used to analyze the Local Level system under various operating conditions and with different component errors such as accelerometer biases and gyroscope drifts. Throughout this analysis a normal gravity field with no anomalous gravity is assumed for the earth. It is envisioned that the anomalous field will be included in the simulation to make the analysis of system errors under even more realistic conditions possible. This may eventually

lead to a priori modeling of the earth's gravity field to improve the system accuracy.

The quality of the output data from the Local Level inertial survey system simulation is provided by Kalman filtering techniques derived in this study. The simulation results presented are based on a seven element state vector which excludes accelerations in the vertical channel. The Kalman state vector developed in this study contains three misorientation elements, two horizontal position elements (geodetic latitude and longitude), and two velocity elements. The simulation results indicate that an inertial survey system must have the position, velocity, and orientation errors bounded by using either the Kalman update procedure (Section 4.2) or a simple zero velocity update procedure (Section 3.6). If the component errors are not bounded, the positional errors are totally unacceptable after a one hour simulation run. The two procedures for bounding the errors mentioned above are shown to be equivalent by the simulation results of Section 5.3. However, the major advantage of the Kalman procedure is the provision of accuracy estimates of the computed position, velocity and orientation of the inertial device.

TABLE OF CONTENTS

	Page
ABSTRACT	ii
LIST OF FIGURES	vi
LIST OF TABLES	viii
ACKNOWLEDGEMENTS	ix
1. INTRODUCTION	1
2. BASIC CONCEPTS	4
2.1 Coordinate Frames	4
2.1.1 Inertial Frame	4
2.1.2 Earth Frame	9
2.1.3 Local Level Frame	12
2.2 Normal Gravity Field	14
2.3 Description of Inertial Survey System Components	14
2.3.1 Accelerometer	14
2.3.2 Gyroscope	18
2.4 Types of Inertial Systems	21
3. MECHANIZATION	26
3.1 Derivation of General Equations	26
3.2 Rotating Earth Formulation	30
3.3 Local Level Formulation	32
3.4 Mechanization of Local Level System	38
3.5 Platform Alignment	42
3.6 Zero Velocity Update	43

4.	KALMAN FILTERING	47
4.1	Kalman Filtering	47
4.2	Kalman Filtering Expressions for Local Level Mechanization	52
5.	LOCAL LEVEL SIMULATION	68
5.1	General Flowchart	68
5.2	Position Errors Caused by Accelerometer Biases and Gyro Drifts	79
5.2.1	Accelerometer Biases in the Stationary Mode	79
5.2.2	Gyro Drifts in the Stationary Mode	85
5.2.3	Accelerometer Biases in the Moving Mode	89
5.2.4	Gyro Drifts in the Moving Mode	90
5.3	Zero Velocity Update Simulation	94
5.3.1	Simple ZUPT in the Stationary Mode	94
5.3.2	Simple ZUPT in the Moving Mode	97
5.3.3	Kalman ZUPT in the Stationary Mode	100
5.3.4	Kalman ZUPT in the Moving Mode	105
5.3.5	Time Interval Between ZUPT's	107
6.	CONCLUSIONS AND RECOMMENDATIONS	110
	REFERENCES	115
	APPENDIX I - NOMENCLATURE	117
	APPENDIX II - ROTATION MATRICES	120

LIST OF FIGURES

		Page
Figure 2-1	Coordinate Frames	5
Figure 2-2	Accelerometer and its Response to Applied Force . .	15
Figure 2-3	Accelerometers and Gyroscopes on Platform	17
Figure 2-4	Gyro Response	17
Figure 2-5	Single Degree of Freedom Gyro	20
Figure 2-6	Platform Suspension	23
Figure 3-1	Rotating Sensor Axes	28
Figure 3-2	Mechanization Overview	38
Figure 3-3	Local Level Mechanization	40
Figure 3-4	Velocity Error/Time Curve	44
Figure 4-1	Transition Matrix	63
Figure 5-1	System Flowchart	69
Figure 5-2	Accelerometer Biases - Latitude Error - Stationary Mode	82
Figure 5-3	Accelerometer Biases - Longitude Error - Stationary Mode	83
Figure 5-4	Accelerometer Biases - Height Error - Stationary Mode	84
Figure 5-5	Gyro Drifts - Latitude Error - Stationary Mode .	86
Figure 5-6	Gyro Drifts - Longitude Error - Stationary Mode .	87
Figure 5-7	Gyro Drifts - Height Error - Stationary Mode . .	88
Figure 5-8	Accelerometer Biases - Latitude Error - Moving Mode	91
Figure 5-9	Accelerometer Biases - Longitude Error - Moving Mode	91

	Page
Figure 5-10	Accelerometer Biases - Height Error - Moving Mode 92
Figure 5-11	Gyro Drifts - Latitude Error - Moving Mode 92
Figure 5-12	Gyro Drifts - Longitude Error - Moving Mode . . . 93
Figure 5-13	Gyro Drifts - Height Error - Moving Mode 93
Figure 5-14	Longitude Standard Deviation vs Time For Different Zupt Intervals 108

LIST OF TABLES

	Page
Table 5-1	Traverse Points 89
Table 5-2	Simple ZUPT - Latitude Error - Stationary Mode . . 95
Table 5-3	Simple ZUPT - Longitude Error - Stationary Mode . 96
Table 5-4	Simple ZUPT - Height Error - Stationary Mode 96
Table 5-5	Elapsed Time - Distance Traversed - Moving Mode . . 98
Table 5-6	Simple ZUPT - Latitude Error - Moving Mode 98
Table 5-7	Simple ZUPT - Longitude Error - Moving Mode 99
Table 5-8	Simple ZUPT - Height Error - Moving Mode 100
Table 5-9	Kalman ZUPT - Latitude and Longitude Error - Stationary Mode 103
Table 5-10	Latitude and Longitude Standard Deviation - Stationary Mode 105
Table 5-11	Kalman ZUPT - Latitude and Longitude Error - Moving Mode 106
Table 5-12	Latitude and Longitude Standard Deviation - Moving Mode 107

ACKNOWLEDGEMENT

The first acknowledgement must go to my knowledgeable advisors Dr. D. B. Thomson and Dr. K.P. Schwarz, who through their constructive criticism and contribution of their valuable time have made this work possible.

I would also like to thank Natural Sciences and Engineering Research Council Canada, and Energy Mines and Resources Canada for their financial assistance given while preparing this report. Mrs. K. Ellerton is acknowledged for her patience and dedication in the typing of this report and Mr. S. MacRitchie is acknowledged for his excellent drafting work.

This report is dedicated to my wife Moyra for her patience, support, and understanding and also to my parents for their never ending faith.

1. INTRODUCTION

Inertial navigation systems have existed for some years and may be readily found in aircraft, submarines, missiles, ships and many land vehicles. The technological advances since the second World War have recently made the use of these systems possible for surveying measurements. To accomplish this, systems with accuracies in the nautical mile range have had to be modified to obtain accuracies of less than ten metres. This involved not only the modification of the equipment, but also a reevaluation of the mechanization equations and operating procedures. The main objective of this report is to describe and evaluate the Local Level inertial survey system presently being used by the surveying industry.

Because of the complexity of the inertial system, the first topic dealt with in this report is the presentation of the basic concepts. Here, the use of Newtonian mechanics is explained and the time system and various coordinate frames are defined. The fundamental components of the system, namely the gyroscope and the accelerometer, are briefly examined. Following this, the different types of inertial survey systems which may be constructed are described conceptually.

The next major topic concerns the mechanization equations. In this section the general mechanization equations are derived.

These equations enable the various inertial survey systems to separate the actual acceleration in the chosen coordinate frame from the accelerations sensed. For the Local Level system this implies the elimination of the gravitational attraction of the earth, centrifugal acceleration, centripetal acceleration, and tangential acceleration. In this section, the general equations mentioned above are used to derive the Local Level mechanization equations and also the Rotating Earth equations. After the derivation, the mechanization flowchart, platform alignment, and a simple form of zero velocity updating, are examined. It is partly because of this zero velocity updating procedure that survey accuracies have been obtainable.

The inertial survey system is, as previously mentioned, a very complex instrument with many error sources. This, coupled with the fact that the inertial survey systems are dynamic, have led to the use of Kalman filtering techniques for the determination of the state vector corrections and their associated accuracies. The fourth section of this report describes the general Kalman equations and the Kalman expressions are developed for a special case of the Local Level system in which the state vector contains three misorientation errors, two position errors, and two velocity errors.

The final stage of this report involves the computer simulation of the Local Level inertial survey system. To be able to see how certain biases and approximations affect the output of the inertial system a computer program was developed and the numerical results from this program are presented in Section 5. The simulation program enables the user to evaluate the Kalman filter derivations before their implementation in the actual system. This eliminates the

need for using the actual inertial system for time consuming tests, and also enables a better quality control of the testing. Eventually it is hoped that the simulation program will also be used to design a practical method of eliminating the systematic errors introduced by the anomalous gravity field, as well as the systematic errors introduced by the mechanical inadequacies of the system.

2. BASIC CONCEPTS

Inertial technology is relatively new to the surveying engineering discipline and it is therefore necessary to set up a firm base from which to begin investigations. Before considering the details of the commonly used Local Level inertial survey system, and its simulation, some basic definitions and explanations of terminology peculiar to inertial technology must be given.

2.1 Coordinate Frames

Before beginning any description of inertial survey systems, the coordinate frames and the transformations between them must be stated. All of the frames given here are orthogonal and right handed.

2.1.1 Inertial Frame

The Inertial frame, Figure 2-1, is the first to be considered. Greenwood [1965] defines the Inertial or Newtonian frame to be "... any rigid set of coordinate axes such that particle motion relative to these axes is described by Newton's laws of

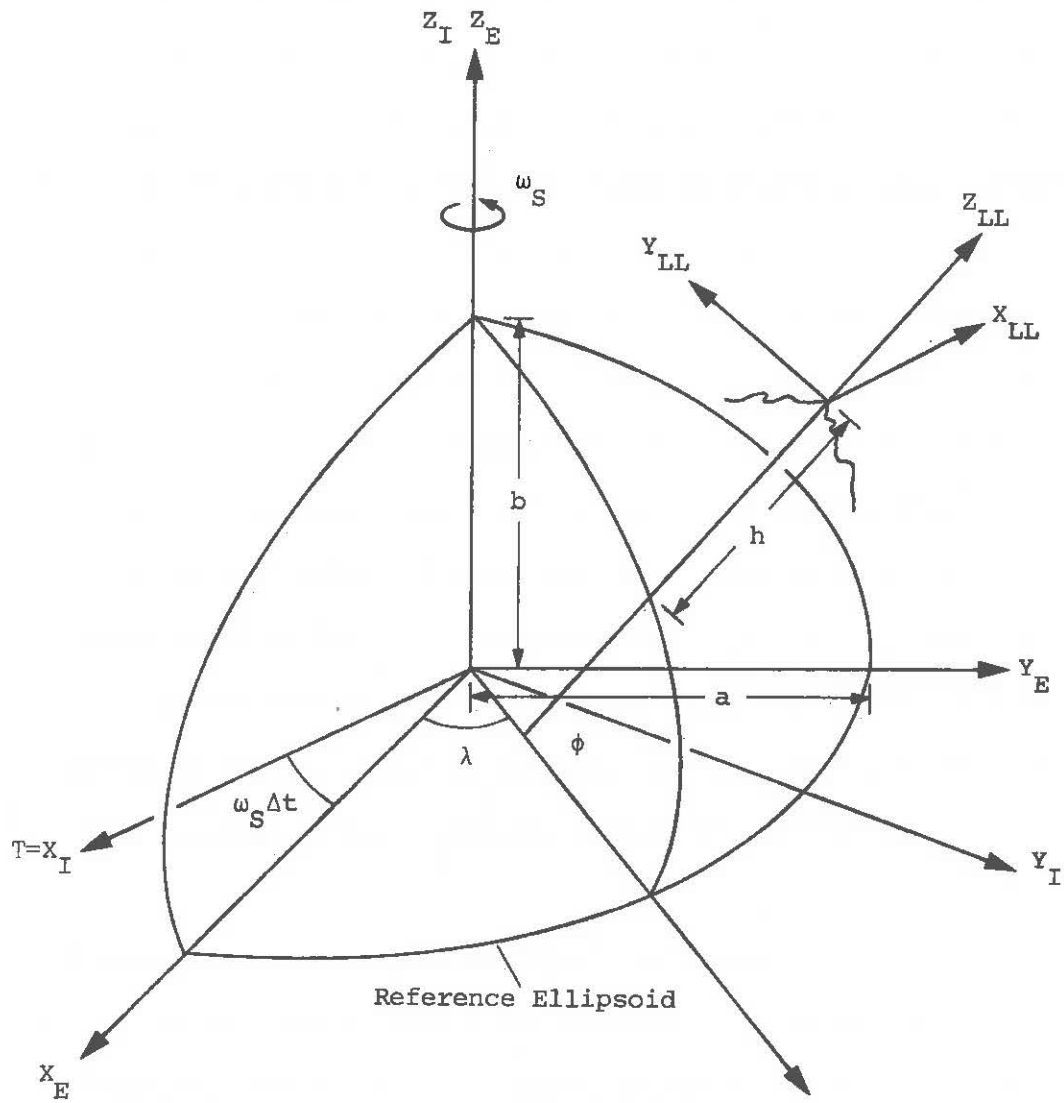


Figure 2-1
Coordinate Frames

motion.", and goes further to say that "It can be shown that any other reference frame that is not rotating but is translating with a uniform velocity relative to an inertial frame is itself an inertial frame.". Since Newtonian mechanics are used throughout this report a convenient inertial frame which can be related to the sensitive axes of an inertial survey system must be found. The usual procedure is to define an approximate inertial frame in such a way that the errors caused by the definition are below the sensitivity of the system sensors. The Inertial frame chosen is one with its origin at the instantaneous center of gravity of the earth. The Z_I axis is coincident with the Instantaneous Terrestrial rotation axis. The X_I axis is oriented to the instantaneous vernal equinox, T , which is the line of intersection of the true ecliptic plane and the true celestial equator. The Y_I axes completes the frame so that it is right handed. The above definition is identical to that of the Apparent Place coordinate system given in Krakiwsky and Wells [1971]. The frame will be referred to as the Inertial frame throughout this report.

The Inertial frame just described is not fixed in inertial space. The true celestial equator is not a fixed plane; it is subject to precession, nutation, and polar motion. Kayton [1960] estimates the inertial angular velocity normal to the instantaneous spin axis resulting from precession and nutation is less than 10^{-6} degrees per hour. He also estimates that the angular velocity resulting from polar motion has a value of approximately 5×10^{-5} degrees per hour. When assuming gyro drift rates of .0004 degrees per hour [Hadfield, 1977] for current conventional spin gyroroscopes, the above angular

velocities are not significant. Therefore, the mechanization equations (Section 3.1) do not take these angular velocities into account.

Implicit in the definition of an inertial frame is the choice of a time scale. When dealing with inertial systems the time interval and not the time epoch is of primary importance. It is with respect to the chosen time interval that the numerical integration takes place in an inertial system. One of the best time interval scales is the atomic time scale based on the electromagnetic oscillations produced by the quantum transition of the cesium-133 atom [Mueller, 1969]. The difference between the atomic second and the ephemeris second used by astronomers is in the order of 2×10^{-9} for a one second interval [Mueller, 1969]. The ephemeris time scale is implied throughout this report.

The spin rate of the earth is defined in terms of ephemeris seconds. The inertial day based on transits of the fixed stars is found to be 86164.10 ephemeris seconds. This spin rate is a mean value and the fluctuations in the rate must be examined. Vanicek and Krakiwsky [in prep.] state that the rotation rate appears to be decreasing at a rate of 1.6 ms per century. This decrease is well below the current inertial sensor sensitivity and need not be considered. The short term fluctuation of the earth rate may be as high as 10 ms per day [Vanicek and Krakiwsky, in prep.]. This would cause an error in platform orientation of approximately 1.5×10^{-4} arc seconds per day and with gyroscope drifts in the order of 36 arc seconds per day need not be considered in the mechanization, Section 3. The centrifugal force at the equator caused by a variation of 10 ms per day in the spin rate would be in the order of 1×10^{-11} m/sec² which is well below the current acceleration measuring sensitivity of 1×10^{-5} m/sec²

[Huddle, 1977].

Having decided on the origin of the Inertial frame, its orientation in inertial space, the type of time scale and its relationship to the angular velocity of the earth, the gravitational attraction of the other bodies in the universe must be considered. The implicit assumption thus far has been that the earth is in a state of free fall and therefore the acceleration of the earth's center of gravity is equal and opposite to the gravitational attractions that caused the earth's movement; hence an acceleration measuring device located at the center of gravity of the earth would not detect any accelerations. The acceleration measurements for terrestrial inertial systems are made on the earth's surface and the gravitational variations of the largest influences, the moon and sun should be examined. A simple method of examining the variation in gravitational attraction on opposite sides of the earth is to take the derivative of the gravitational attraction with respect to the radius which yields

$$\Delta F = \frac{\kappa M}{r^3} \Delta r \quad , \quad (2-1)$$

where ΔF is the variation in gravitation κ is the gravitational constant, $6.672 \times 10^{-14} \text{ m}^3 \text{ s}^{-2} \text{ kg}^{-1}$, M is the mass of the moon or sun, Δr is the approximate diameter of the earth, and r is the mean distance from the moon to the earth or from the sun to the earth. Using equation (2-1) and the appropriate values, the gravitational variation of the moon is approximately 0.11 milligals, and that of the sun is approximately 0.05 milligals. The current acceleration sensors have a sensitivity of one milligal and hence would not be able to detect the combined gravitational variation of 0.16 milligals.

Because the inertial measurements are made on the earth's surface, the next step is to define coordinate frames which may be instrumented there and then show their relationship to the Inertial frame just described.

2.1.2 Earth Frame

The Earth frame, Figure 2-1, or as it is often called the Instantaneous Terrestrial frame [e.g. Krakiwsky and Wells, 1971], is fixed within the earth. The origin is the center of gravity of the earth. The Z_E axis coincides with the earth's instantaneous rotation axis. The X_E axis is the intersection of the earth's instantaneous equatorial and Greenwich Astronomic Meridian planes. The Y_E axis completes the frame so that it is right handed. The angular velocity of the Earth frame with respect to the inertial frame is

$$\vec{\omega}_E = \begin{bmatrix} 0 \\ 0 \\ \omega_S \end{bmatrix}, \quad (2-2)$$

where ω_S is the angular velocity of the earth. Using the previously defined value for the length of a day, the value for ω_S is

$$\begin{aligned} \omega_S &= 2\pi/86164.10 \\ &= 7.2921151 \times 10^{-5} \text{ rad sec}^{-1}. \end{aligned} \quad (2-3)$$

The transformation from the Earth frame to the Inertial frame is given by (Figure 2-1)

$$\begin{bmatrix} X \\ Y \\ Z \end{bmatrix}_I = R_3(-\omega_S \Delta t) \begin{bmatrix} X \\ Y \\ Z \end{bmatrix}_E, \quad (2-4)$$

where the rotation matrix convention is as described in Appendix II and Δt is the elapsed time from the instant when the X_E axis was coincident with the X_I axis and is measured in ephemeris seconds.

In Figure 2-1, geodetic latitude ϕ , longitude λ , and height h are illustrated. The relationship between these coordinates and the three dimensional Cartesian coordinates of the same point in an Earth frame is [e.g. Krakiwsky and Wells, 1971]

$$\begin{bmatrix} X \\ Y \\ Z \end{bmatrix}_E = \begin{bmatrix} (N+h) \cos \phi \cos \lambda \\ (N+h) \cos \phi \sin \lambda \\ (Nb^2/a^2 + h) \sin \phi \end{bmatrix}, \quad (2-5)$$

where a is the semi-major axis of the geocentric reference ellipsoid, b is the semi-minor axis of the geocentric reference ellipsoid, and N is the prime vertical radius of curvature given by

$$N = a / (1 - e^2 \sin^2 \phi)^{1/2} \quad (2-6)$$

Another radius which will be required is M , the meridian radius of curvature given by

$$M = a(1 - e^2) / (1 - e^2 \sin^2 \phi)^{3/2}, \quad (2-7)$$

where e is the first eccentricity,

$$e = ((a^2 - b^2)/a^2)^{1/2}. \quad (2-8)$$

For the inverse transformation of (2-5) the interested reader is referred to, for example, Krakiwsky and Wells [1971].

The reference ellipsoid which will be used for this study is the geocentric ellipsoid adopted by the International Union of Geodesy and Geophysics in 1967 at Moscow which has the parameters

$$a = 6\,378\,160.0 \text{ metres}, \quad (2-9)$$

and

$$b = 6\,356\,774.516 \text{ metres}. \quad (2-10)$$

The Earth frame that has just been described must also be related to the various systems of geodetic coordinates that have already been established throughout the world. The reason for this is that the inertial system is used to determine position differences in the Earth frame and it requires the coordinates of its starting position in this frame.

Turning to the coordinates of existing networks, the relationship with the Average Terrestrial system may be stated as [e.g. Krakiwsky and Wells, 1971]

$$\begin{bmatrix} X \\ Y \\ Z \end{bmatrix}_{AT} = \begin{bmatrix} \Delta X \\ \Delta Y \\ \Delta Z \end{bmatrix} + \begin{bmatrix} (N+h) \cos \phi \cos \lambda \\ (N+h) \cos \phi \sin \lambda \\ (Nb^2/a^2 + h) \sin \phi \end{bmatrix}, \quad (2-11)$$

where the vector $[\Delta X, \Delta Y, \Delta Z]^T$ is the translation vector from the origin of the Average Terrestrial system to the origin of the coordinate system to which a network refers. The Average Terrestrial coordinates may then be converted to the Earth frame system previously defined, neglecting the migration of the center of gravity of the earth, by the relationship [e.g. Krakiwsky and Wells, 1971]

$$\begin{bmatrix} X \\ Y \\ Z \end{bmatrix}_E = R_1(Y_P) R_2(X_P) \begin{bmatrix} X \\ Y \\ Z \end{bmatrix}_{AT}, \quad (2-12)$$

where X_P and Y_P are the polar motion components. Before beginning inertial system measurements on the surface of the earth, the existing coordinates should be first converted to the Earth frame via equations (2-11) and (2-12).

2.1.3 Local Level Frame

Before defining the Local Level frame a few points should be noted. This study neglects the anomalous gravity field of the earth and the development that follows is for a system that can maintain a Local Level orientation. In reality the Local Level inertial system initially aligns itself in the Local Astronomic frame. This misalignment through the deflection of the vertical and the anomalous gravity field introduce significant errors [Macomber, 1966], but their inclusion is beyond the scope of this report. Also, because normal gravity is assumed throughout this report, the 1967 International ellipsoid is oriented so that the semi-minor axis of the ellipsoid coincides with

the Z_E axis of the Earth frame, instead of the Average Terrestrial Z_{AT} axis (no polar motion components).

The Local Level frame, Figure 2-1, is defined to have its origin at the point where the inertial measurements are being made. The Z_{LL} axis is coincident with the ellipsoidal normal. The Y_{LL} axis is directed towards the instantaneous rotation axis of the earth (Z_E axis). The X_{LL} axis is oriented to complete the right handed system. The relationship between the Local Level and the Earth frame is

$$\begin{bmatrix} X \\ Y \\ Z \end{bmatrix}_E = R_3(-90 - \lambda) R_1(\phi - 90) \begin{bmatrix} X \\ Y \\ Z \end{bmatrix}_{LL} \quad (2-13)$$

The relationship of the Local Level and Inertial frames is easily obtained by combining (2-13) and (2-4) which results in

$$\begin{bmatrix} X \\ Y \\ Z \end{bmatrix}_I = R_3(-\omega_S \Delta t) R_3(-90 - \lambda) R_1(\phi - 90) \begin{bmatrix} X \\ Y \\ Z \end{bmatrix}_{LL} \quad (2-14)$$

The angular velocity of the Local Level frame with respect to the Inertial frame is given by

$$\vec{\omega}_{LL} = \begin{bmatrix} -\dot{\phi} \\ (\omega_S + \dot{\lambda}) \cos \phi \\ (\omega_S + \dot{\lambda}) \sin \phi \end{bmatrix} \quad (2-15)$$

where $\dot{\phi}$ is the change in latitude with time (latitude velocity) and $\dot{\lambda}$ is the change in longitude with time (longitude velocity).

2.2 Normal Gravity Field

As was previously mentioned (2.1.3) the assumption made for this study is that the inertial measurements are made in a normal gravity field. Normal gravity (γ) at any point on or above the reference ellipsoid is expressed, as [International Association of Geodesy, 1967]

$$\gamma = 978.031\ 85(1 + .005\ 278\ 895\ \sin^2\phi + .000\ 023\ 462\ \sin^4\phi) - .308\ 6 \times 10^{-3}h, \quad (2-16)$$

in units of gals (for h expressed in metres). The above formula approximates normal gravity on the reference ellipsoid with an accuracy of 4×10^{-6} gals. The formula is derived from other constants specified by the International Association of Geodesy [1967]. The term involving h in equation (2-16) accounts for the vertical gradient of gravity and is sometimes referred to as the free air correction [Heiskanen and Moritz, 1967]. The term "free air" makes reference to the fact that there is assumed to be no mass between the ellipsoid and the observation point.

2.3 Description of Inertial Survey System Components

2.3.1 Accelerometer

The basic process behind inertial surveying is the double integration of measured accelerations to obtain a change of position. The device used to measure accelerations is termed an accelerometer. The accelerometer could be a restrained sliding mass, Figure 2-2a, pendulum,

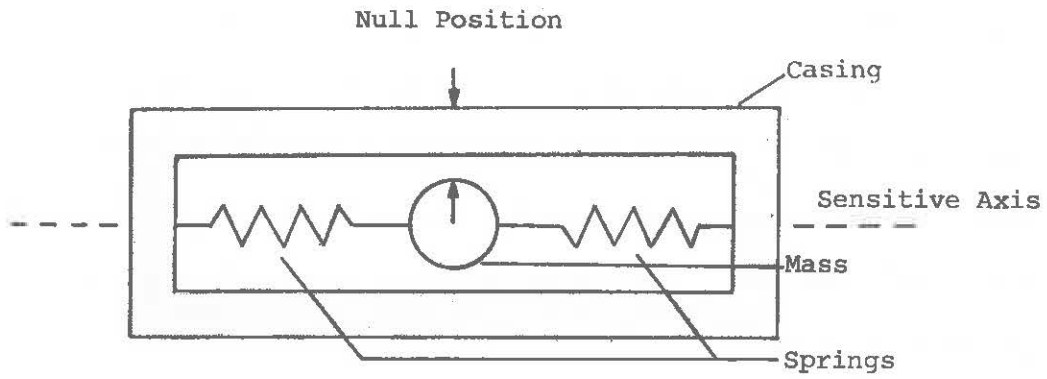


Figure 2-2a
Accelerometer

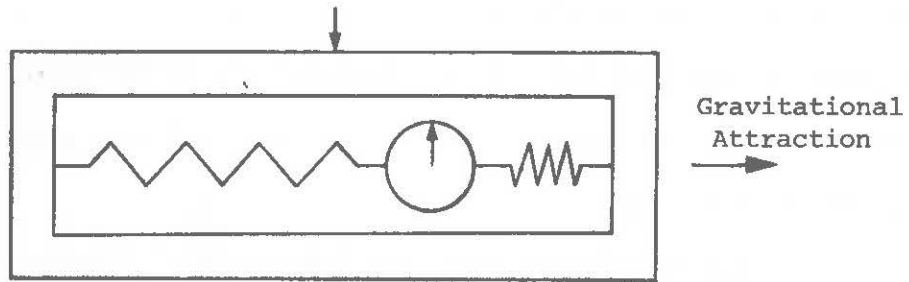


Figure 2-2b
Gravitational Response

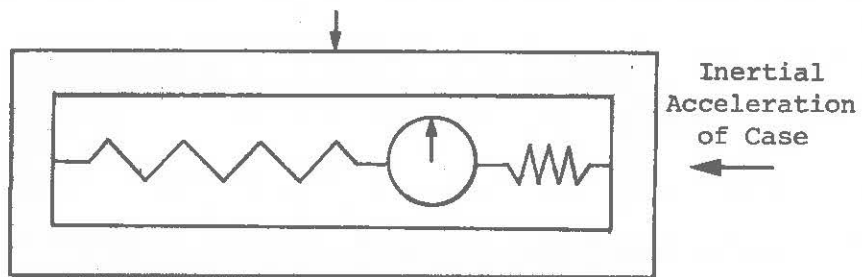


Figure 2-2c
Inertial Acceleration Response

Figure 2-2
Accelerometer and its Response to Applied Force

or a more sophisticated device but the basic principle remains the same. Figure 2-2b and Figure 2-2c illustrate the basic accelerometer response to an applied force. By measuring the amount of mass displacement, and realizing that the displacement is directly proportional to the applied force, one may compute the sensed acceleration along the sensitive axis. The final conversion formula is the result of a factory calibration of the accelerometer.

The acceleration indicated by the accelerometer could be the result of gravitational attraction, Figure 2-2b, or other forces such as Coriolis, centripetal or tangential force as well as acceleration in inertial space, Figure 2-2c. Section 3 shows the development for separating out the acceleration in the desired frame from the various sensed accelerations.

Once an accelerometer has been properly calibrated the **uncertainty (noise)** in the acceleration measurement should be in the order of 1 milligal [Huddle, 1977]. This can be readily compared to a Gravimeter, which is another application of an accelerometer, which has an uncertainty of .01 milligals.

Because the accelerometer, Figure 2-2a, detects applied forces along its sensitive axis only, three such accelerometers must be utilized to detect applied forces in three dimensions. These accelerometers are orthogonally mounted on a base or platform, Figure 2-3. If the orientation of the platform with respect to some coordinate frame is known then it would be possible to separate out the acceleration in that frame, and then double integrate to obtain the change in position.

The obvious problem is how to insure the orientation of this platform in space. This is done via gyroscopes which are described

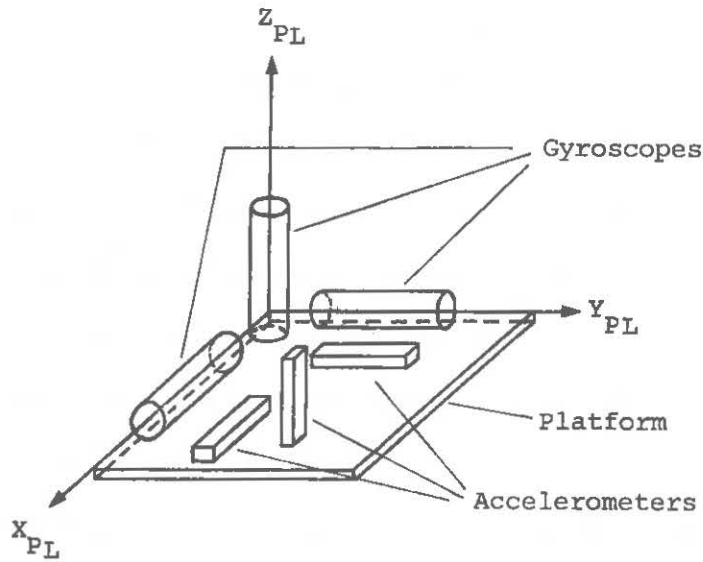


Figure 2-3
Accelerometers and Gyroscopes on Platform

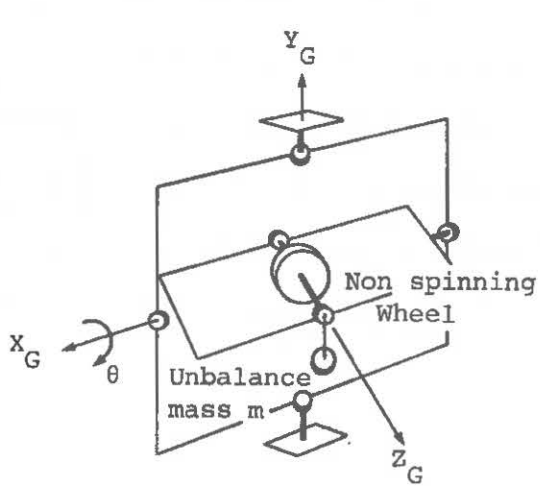


Figure 2-4a
Torque applied - non-spinning

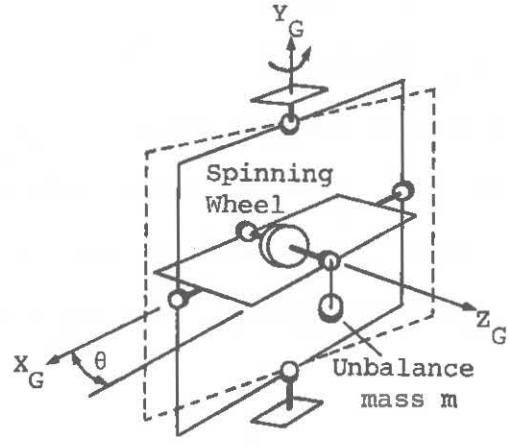


Figure 2-4b
Torque applied - spinning

Figure 2-4
Gyro Response

in the next section.

2.3.2 Gyroscope

The study of a gyroscope, hereafter to be called simply gyro, and its properties is a science in itself and no attempt is made here to give an in-depth description of it. The main characteristic that makes the gyro a useful tool is its precession under the effect of an applied torque. This is best explained with the aid of an illustration, Figure 2-4. Considering Figure 2-4a, with the non-spinning wheel, one sees that the effect of the torque generated by the unbalance mass m is to rotate the structure of gimbals about the X_G axis in the direction indicated by θ . Turning to Figure 2-4b it is seen that the same torque about the X_G axis, input axis, of the spinning wheel causes a rotation about the Y_G axis, output axis, by an amount indicated by θ . The remaining axis, Z_G , is usually referred to as the spin axis. It can be shown [Greenwood, 1965] that the application of a torque to the spin axis causes the axis to deflect at right angles to the plane in which the torque is applied and the relationship is expressed mathematically as [Farrell, 1976]

$$L = H \dot{\beta} \quad (2-17)$$

where L is the gyroscopic moment (torque developed), H is the angular momentum of the rotor and $\dot{\beta}$ is the applied torque about the input axis.

The situation depicted in Figure 2-4b is that of a gyro with two degrees of freedom. To explain the use of the gyro in inertial

surveying applications, use will be made of the single degree of freedom (S.D.F.) gyro. It should be noted that 2 two degree of freedom gyros are equivalent to 3 S.D.F. gyros, with the redundancy of the two degree of freedom gyros being used in the desired channel. Considering Figure 2-5, it can be seen that the only rotation possible for the S.D.F. gyro is about the Y_G axis. This rotation would be caused by a rotation of the platform base about the input axis X_G . One could compute a restraining torque $\dot{\theta}$ to offset the displacement caused by the $H\dot{\beta}$ term in equation (2-17) to obtain the net torque about the output axis as

$$L = H\dot{\beta} - B\dot{\theta} , \quad (2-18)$$

where B is a proportionality constant. A first approximation to the rate integrating gyro neglects the net torque in (2-18) to yield

$$H\dot{\beta} = B\dot{\theta} . \quad (2-19)$$

Integrating yields

$$\beta/\theta = B/H . \quad (2-20)$$

Using a gyro pickoff, Figure 2-5 one could measure the angle θ , then using the relationship (2-20) solve for the rotation β of the platform with respect to the Inertial frame. To complete the gyro principles the use of the gyro torquer in Figure 2-5 must be explained. The torquer is used to torque the gyro about the output axis so that

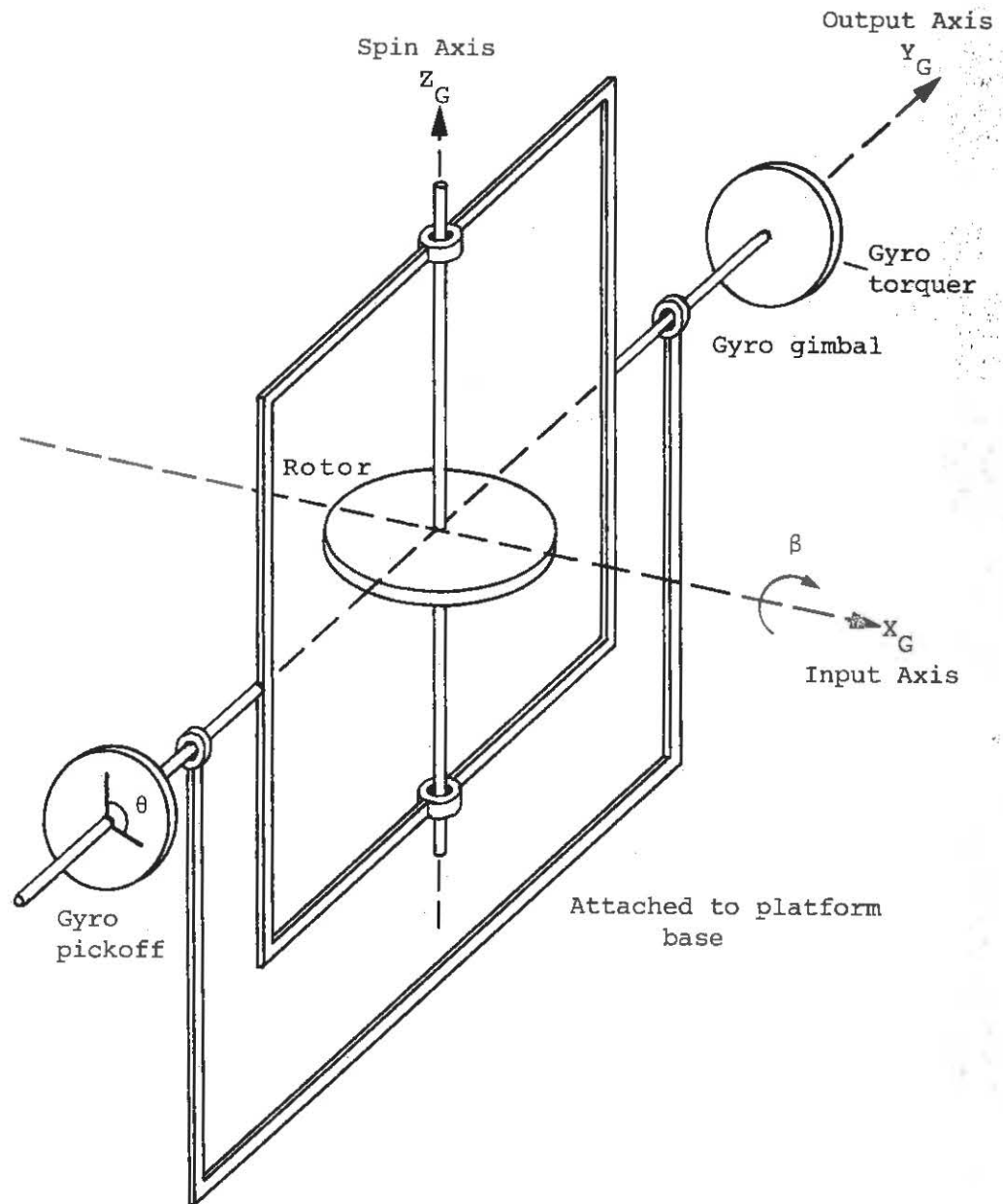


Figure 2-5
Single Degree of Freedom Gyro

the gyro spin axis maintains the desired orientation in inertial space. To maintain orientation in three-dimensional space three such S.D.F. gyros must be mounted on the platform, Figure 2-3. The gyros are mounted orthogonally and their orientation with respect to the accelerometer triad is known. It is the orientation of the platform, and hence the accelerometer triad, that determines the type of inertial system.

2.4 Types of Inertial Systems

The first system to be examined is the Strapdown system. In this system the platform, Figure 2-3, is strapped or fixed to the frame of the vehicle. In the Strapdown system only the gyro pickoffs are theoretically necessary but in practice the gyro torquers are needed to align the platform, eliminate gyro drift, and in certain gyro arrangements null the gyro pickoff angle after each measurement. The recorded change in orientation of the platform is all that is needed to compute proper vehicle velocities and positions. Before the advent of laser gyros [Savage, 1978], the dynamic-range problems of conventional spin gyros made the strapdown configuration unsuitable for even navigational purposes. Strapdown systems are now becoming feasible however, and are being used more and more in the navigation industry. The big advantage of Strapdown systems, using laser gyros, is the lack of moving parts. The disadvantage is the increased complexity of the computations, but with the advent of micro chip computer technology this no longer appears to be a problem. There are no Strapdown systems being used for surveying applications at the present time but the interested reader is referred to, for example, Farrell [1976]

or VanBronkhorst [1978].

The platform could also be put on a gimballed structure as indicated in Figure 2-6. This gimballed platform gives one the flexibility to instrument virtually any desired frame. The gimbals provide the platform with a great deal of isolation from the vehicle angular velocity but torques of the platform do occur. Figure 2-6 illustrates a platform with three sets of gimbals whereas on actual systems there is a fourth set which is used to prevent gimbal lock as explained in Farrell [1976].

Using the gimballed platform, the instrumenting of the Space Stabilized system, in which the sensors have a fixed orientation with respect to the Inertial frame, is perhaps the easiest to comprehend. In this system the only torquing theoretically required is that done by the torquing motors, Figure 2-6, of the platform, but again in practice the gyro torquers are needed to help align the platform, and for certain gyro arrangements null the gyro pickoff angle after each measurement, and eliminate gyro drift. If an angular velocity is sensed by the gyro pickoffs, see Figure 2-5, then a signal is sent to the appropriate platform gimbal torquer and the platform is returned to its original orientation in the Inertial frame. The appropriate gimbal torquer is that one which rotates the platform about the input axis of the gyro that sensed the change in orientation.

The next system examined is the Rotating Earth system whose platform is given the same angular velocity as that of the earth. Consider the case where the three gyro input axes and three sensitive accelerometer axes are nominally parallel to the Earth frame. To maintain the platform in this orientation the signal from the gyro which has its input axis parallel to the rotation axis of the earth,

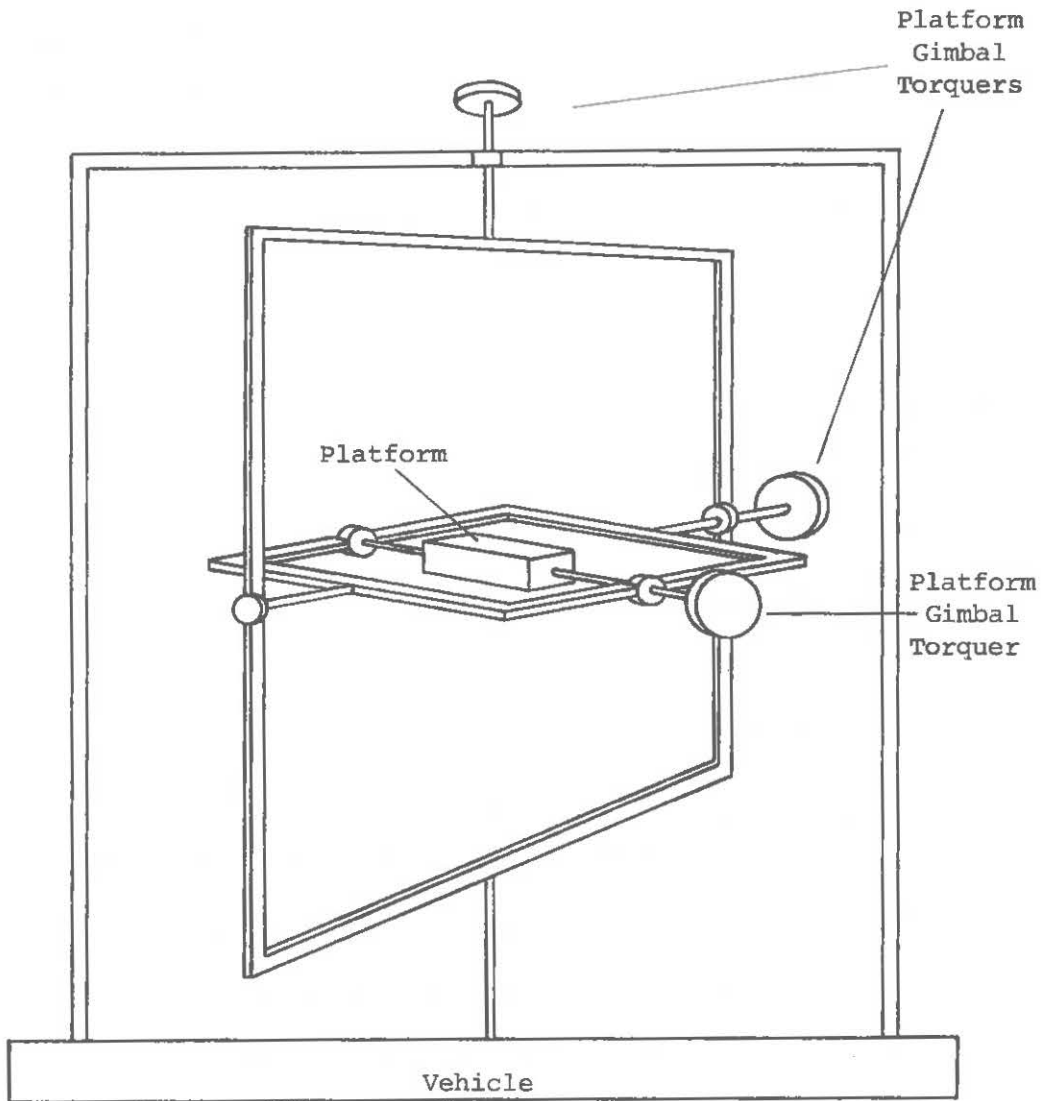


Figure 2-6
Platform Suspension

Z_E must include the angular velocity ω_S . This implies that this gyro must be torqued by the amount (from equation 2-17)

$$L = H\omega_S \quad , \quad (2-21)$$

so that the signal at the gyro pickoff which will be sent to the platform gimbal axis, which is parallel to Z_E , is equal to the earth rate. Combining (2-21) with (2-18) yields

$$\dot{B\theta} = H\dot{\beta} + H\omega_S$$

or rewriting

$$\dot{\beta} = (\dot{B\theta} - H\omega_S)/H \quad (2-22)$$

Integrating the above one obtains

$$\beta = (B\theta - H\omega_S \Delta t)/H \quad (2-23)$$

where Δt is the elapsed time and β is the net amount by which the platform gimbal parallel to Z_E must be rotated. The above description has been simplified and the real time torquing of the platform is a much more complex problem with many second order effects [Farrell, 1976] which have not been described here. The point to be noted is that the angular velocity of the Rotating Earth platform would be given by equation (2-2) if the system were mechanically perfect.

The system that is of most interest in this study is the Local Level system. Here the three gyro input axes and three sensitive accelerometer axes are nominally aligned with the Local Level frame. To maintain this orientation the platform must be driven at an angular

velocity given by equation (2-15). The torquing commands to the platform gimbals are derived using the same principles as those mentioned in the Rotating Earth system, and the interested reader is referred to Britting [1971] or Farrell [1976] for further information.

Finally it is assumed throughout the remainder of this report that the gyros and accelerometers are perfectly aligned to each other, and that they are orthogonal. These assumptions are definitely approximations but there is a lack of literature on the non-orthogonality and calibration theory to state precisely the limitations in this area for inertial survey systems.

3. MECHANIZATION

In the previous section the various coordinate frames have been defined and the basic sensors described. The objective of this section is to derive the basic mechanization equations, assuming Newtonian mechanics, for the Rotating Earth and Local Level inertial systems. The Rotating Earth system is included because it is in this frame that the data is generated for the simulation program described in Section 5.

The general mechanization equations for any chosen measuring frame are derived first, and these equations are then implemented to obtain the equations for the Rotating Earth and Local Level formulations.

3.1 Derivation of General Equations

Consider the position vector of a point in an Inertial frame as

$$\vec{r}_I = X\vec{i}_I + Y\vec{j}_I + Z\vec{k}_I \quad , \quad (3-1)$$

where \vec{i}_I , \vec{j}_I , and \vec{k}_I are the unit vectors along the Inertial axes.

The time derivative of equation (3-1) yields the velocity, namely

$$\vec{r}_I = \dot{X}\vec{i}_I + \dot{Y}\vec{j}_I + \dot{Z}\vec{k}_I \quad (3-2)$$

and the second derivative yields the acceleration in an Inertial frame as

$$\ddot{\vec{r}}_I = \ddot{X}\vec{i}_I + \ddot{Y}\vec{j}_I + \ddot{Z}\vec{k}_I \quad (3-3)$$

If Inertial frame positions were required the position computation, assuming constant acceleration over each small time interval Δt , would be

$$\vec{r}_I(i+1) = \vec{r}_I(i) + \dot{\vec{r}}_I(i)\Delta t + \frac{1}{2}\ddot{\vec{r}}_I(i, i+1)\Delta t^2 \quad (3-4)$$

The inclusion of the gravitation term and the conversion of the Inertial frame coordinates to the Earth frame coordinates through the application of the inverse of equation (2-4) would solve the problem of positioning on the surface of the earth. However, the measurements are usually performed in a non-inertial frame. The sensors, gyros and accelerometers, in the Rotating Earth system and the Local Level system have an angular velocity with respect to the Inertial frame and therefore a more general approach must be taken to solve the mechanization problem.

To begin the general case consider Figure 3-1. The absolute velocity of the point P, coordinated in the sensor axes (X_{SA}, Y_{SA}, Z_{SA}) , would be [Greenwood, 1965]

$$\vec{v}_{SA} = \dot{\vec{r}}_{SA} + \vec{\omega}_{SA} \times \vec{r}_{SA} \quad (3-5)$$

where

\vec{v}_{SA} = absolute velocity in Inertial frame coordinated
in the sensor axes directions,

$\dot{\vec{r}}_{SA}$ = velocity of the point P relative to the
rotating sensor axes,

$\vec{\omega}_{SA}$ = angular velocity of the rotating sensor axes
with respect to the Inertial frame,

and

\vec{r}_{SA} = position vector of the point P coordinated
in the frame indicated by the sensor axes
(e.g. Rotating Earth or Local Level axes).

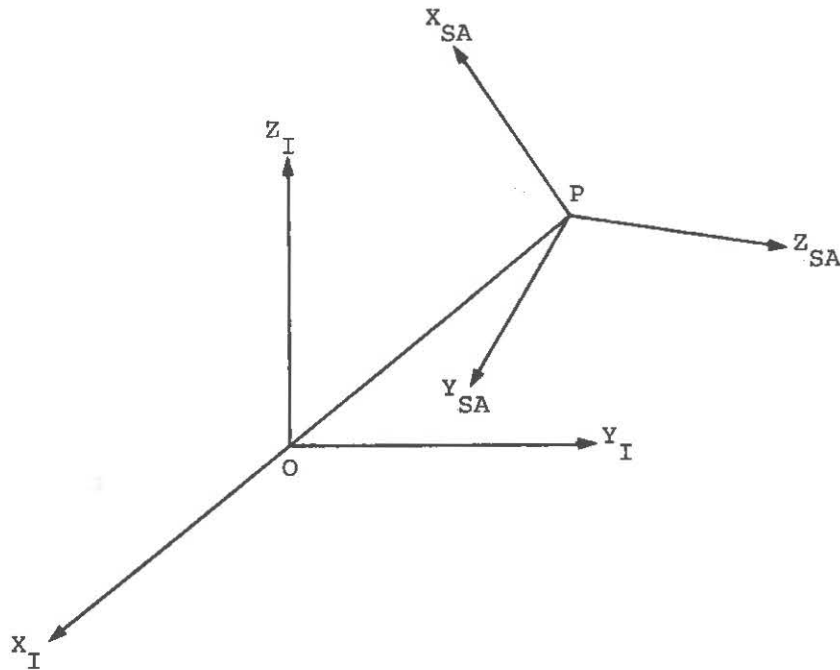


Figure 3-1
Rotating Sensor Axes

To obtain the absolute acceleration the derivative of equation (3-5) is taken to yield [Greenwood, 1965]

$$\vec{a}_{SA} = \dot{\vec{v}}_{SA} + \vec{\omega}_{SA} \times \vec{v}_{SA} \quad (3-6)$$

The first term on the right hand side is given by the time derivative of equation (3-5) namely

$$\dot{\vec{v}}_{SA} = \ddot{\vec{r}}_{SA} + \dot{\vec{\omega}}_{SA} \times \vec{r}_{SA} + \vec{\omega}_{SA} \times \dot{\vec{r}}_{SA} \quad (3-7)$$

and the second term, substituting from (3-5) yields

$$\vec{\omega}_{SA} \times \vec{v}_{SA} = \vec{\omega}_{SA} \times (\dot{\vec{r}}_{SA} + \vec{\omega}_{SA} \times \vec{r}_{SA}) \quad (3-8)$$

Substituting (3-8) and (3-7) into (3-6) gives rise to the final expression

$$\vec{a}_{SA} = \ddot{\vec{r}}_{SA} + 2\vec{\omega}_{SA} \times \dot{\vec{r}}_{SA} + \dot{\vec{\omega}}_{SA} \times \vec{r}_{SA} + \vec{\omega}_{SA} \times \vec{\omega}_{SA} \times \vec{r}_{SA} \quad (3-9)$$

where the second term on the right hand side is often called the Coriolis acceleration, the third term is called tangential acceleration, and the final term is the centripetal acceleration. The \vec{a}_{SA} term in (3-9) is often labelled the absolute acceleration and when the gravitational effects are included it is termed as either the specific force or the sensed accelerations and denoted by f . The general equation (3-9) is now implemented to obtain the absolute accelerations in the Rotating Earth and Local Level inertial systems.

3.2 Rotating Earth Formulation

The first problem will be the application of equation (3-9) for the Rotating Earth system.

Assuming that the axes of the local Rotating Earth system are parallel to the Earth frame axes, then from equation (2-2) the commanded angular velocity of the platform would be

$$\vec{\omega}_{RE} = \begin{bmatrix} 0 \\ 0 \\ \omega_S \end{bmatrix} \quad (3-10)$$

The position vector for a point P on the surface would be

$$\vec{r}_{RE} = \begin{bmatrix} X \\ Y \\ Z \end{bmatrix}_{RE} \quad (3-11)$$

Returning to equation (3-9) it is noted that since the angular velocity (3-10) is considered a constant quantity the term $\dot{\vec{\omega}}_{RE} \times \vec{r}_{RE}$ equals zero. The other terms of equation (3-9) yield

$$2\vec{\omega}_{RE} \times \dot{\vec{r}}_{RE} = \begin{bmatrix} -2\omega_S \dot{Y}_{RE} \\ 2\omega_S \dot{X}_{RE} \\ 0 \end{bmatrix}, \quad (3-12)$$

and

$$\vec{\omega}_{RE} \times \vec{\omega}_{RE} \times \vec{r}_{RE} = \begin{bmatrix} -\omega_S^2 X_{RE} \\ -\omega_S^2 Y_{RE} \\ 0 \end{bmatrix} \quad (3-13)$$

Substituting (3-13) and (3-12) into (3-9) results in

$$\vec{a}_{RE} = \begin{bmatrix} \ddot{X}_{RE} - 2\omega_S \dot{Y}_{RE} - \omega_S^2 X_{RE} \\ \ddot{Y}_{RE} + 2\omega_S \dot{X}_{RE} - \omega_S^2 Y_{RE} \\ \ddot{Z}_{RE} \end{bmatrix} \quad (3-14)$$

To deduce the final specific force equations the gravitational attraction of the earth must be added to the absolute accelerations. The normal gravity, which includes gravitational attraction and centrifugal force, is given in Rotating Earth components as

$$\vec{\gamma}_{RE} = \begin{bmatrix} \gamma \cos \phi \cos \lambda \\ \gamma \cos \phi \sin \lambda \\ \gamma \sin \phi \end{bmatrix}, \quad (3-15)$$

where the term γ is given by equation (2-16). The centripetal components in equation (3-13) can thus be eliminated from (3-14) (since they are included in (3-15)) to yield the specific force equation as

$$\vec{f}_{RE} = \begin{bmatrix} \ddot{X}_{RE} - 2\omega_S \dot{Y}_{RE} + \gamma \cos \phi \cos \lambda \\ \ddot{Y}_{RE} + 2\omega_S \dot{X}_{RE} + \gamma \cos \phi \sin \lambda \\ \ddot{Z}_{RE} + \gamma \sin \phi \end{bmatrix}. \quad (3-16)$$

Implementation of the specific force equation (3-16) would involve obtaining the sensed accelerations from the accelerometers, then using them in equation (3-16) to solve for the accelerations along the Rotating Earth axes. Equations (3-12) and (3-15) are often referred to as the cross product terms. They are not to be confused with the mathematical operator of the same name.

After solving for the Rotating Earth accelerations, the position computations would involve, assuming constant acceleration, an expression similar to equation (3-4), namely

$$\vec{r}_E(i+1) = \vec{r}_E(i) + \dot{\vec{r}}_{RE}(i)\Delta t + \frac{1}{2}\ddot{\vec{r}}_{RE}(i, i+1)\Delta t^2 \quad (3-17)$$

This report does not deal with the position computations using the Rotating Earth system in detail, but as previously mentioned equation (3-14) is needed to generate data for the Local Level system in the simulation program of Section 5.

3.3 Local Level Formulation

The implementation of equation (3-9) in the Local Level system involves some rather long and tedious computations and therefore only the principal expressions will be presented here. A much simpler case develops if a spherical earth is assumed as there is then no need to take derivatives of the radius terms with respect to the latitude. To obtain more information on the spherical simplification reference is made to, for example, Farrell [1976] or Britting [1971].

The angular velocity of the Local Level frame with respect

to the Inertial frame is given using equation (2-15) as

$$\vec{\omega}_{LL} = \begin{bmatrix} -\phi \\ (\omega_S + \dot{\lambda}) \cos \phi \\ (\omega_S + \dot{\lambda}) \sin \phi \end{bmatrix} \quad (3-18)$$

The position vector of a point in terms of the Local Level frame is found by taking the inverse of equation (2-14) to yield

$$\begin{bmatrix} X \\ Y \\ Z \end{bmatrix}_{LL} = R_1(90 - \phi) R_3(90 + \lambda + \omega_S \Delta t) \begin{bmatrix} X \\ Y \\ Z \end{bmatrix}_I \quad (3-19)$$

where the Inertial coordinates expressed in terms of the ellipsoid coordinates are

$$\begin{bmatrix} X \\ Y \\ Z \end{bmatrix}_I = \begin{bmatrix} (N+h) \cos \phi \cos(\lambda + \omega_S \Delta t) \\ (N+h) \cos \phi \sin(\lambda + \omega_S \Delta t) \\ (Nb^2/a^2 + h) \sin \phi \end{bmatrix} \quad (3-20)$$

Substituting (3-20) into (3-19) and evaluating yields

$$\begin{bmatrix} X \\ Y \\ Z \end{bmatrix}_{LL} = \begin{bmatrix} 0 \\ -N \cos \phi \sin \phi e^2 \\ N \cos^2 \phi e^2 + Nb^2/a^2 + h \end{bmatrix} \quad (3-21)$$

Returning to equation (3-9) the various acceleration components may now be solved. The first term on the right hand side of equation (3-9) for the Local Level system yields

$$\ddot{r}_{LL} = \begin{aligned} & 0 \\ & e^2 (N \sin^2 \phi - N \cos^2 \phi - \frac{ae^2 \sin^2 \phi \cos^2 \phi}{Q^3}) \ddot{\phi} \\ & + e^2 (4N \cos \phi \sin \phi - \frac{3ae^2 \sin \phi \cos^3 \phi}{Q^3} \\ & + \frac{3ae^2 \sin^3 \phi \cos \phi}{Q^3} - \frac{3ae^4 \sin^3 \phi \cos^3 \phi}{Q^5}) \dot{\phi}^2 \\ & \ddot{h} + [\frac{ae^2 \sin \phi \cos \phi}{Q^3} (e^2 \cos^2 \phi + \frac{b^2}{a^2}) - 2e^2 N \cos \phi \sin \phi] \ddot{\phi} \\ & + [(e^2 \cos^2 \phi + \frac{b^2}{a^2}) (\frac{ae^2 \cos^2 \phi}{Q^3} - \frac{ae^2 \sin^2 \phi}{Q^3} \\ & + \frac{3ae^4 \sin^2 \phi \cos^2 \phi}{Q^5}) - \frac{2ae^4 \sin^2 \phi \cos^2 \phi}{Q^3} \\ & - 2e^2 N \cos^2 \phi + 2e^2 N \sin^2 \phi - \frac{2e^4 N \cos^2 \phi \sin^2 \phi}{Q^2}] \dot{\phi}^2 \end{aligned} \quad (3-22)$$

where

$$Q = (1 - e^2 \sin^2 \phi)^{1/2} \quad (3-23)$$

The Coriolis term of equation (3-9) for the Local Level system is

$$2\vec{\omega}_{LL} \times \dot{\vec{r}}_{LL} = \begin{bmatrix} 2\ell \cos \phi \left[\dot{h} + \left(\frac{ae^2 \sin \phi \cos \phi}{Q^3} (e^2 \cos^2 \phi + \frac{b^2}{a}) \right) \right. \\ \left. - 2e^2 N \cos \phi \sin \phi \right] \dot{\phi} - 2\ell e^2 \sin \phi \cdot \\ (N \sin^2 \phi - N \cos^2 \phi - \frac{ae^2 \sin^2 \phi \cos^2 \phi}{Q^3}) \dot{\phi} \\ 2\dot{\phi} \left[\dot{h} + \left(\frac{ae^2 \sin \phi \cos \phi}{Q^3} (e^2 \cos^2 \phi + \frac{b^2}{a}) \right) \right. \\ \left. - 2e^2 N \cos \phi \sin \phi \right] \dot{\phi} \\ 2e^2 (N \cos^2 \phi - N \sin^2 \phi + \frac{ae^2 \sin^2 \phi \cos^2 \phi}{Q^3}) \dot{\phi}^2 \end{bmatrix} \quad (3-24)$$

where

$$\ell = \omega_S + \dot{\lambda} \quad (3-25)$$

The tangential acceleration term for the Local Level system is

$$\dot{\vec{\omega}}_{LL} \times \vec{r}_{LL} = \begin{bmatrix} (\ddot{\lambda} \cos \phi - \ell \dot{\phi} \sin \phi) (e^2 N \cos^2 \phi + \frac{Nb^2}{a^2} + h) \\ + e^2 N \cos \phi \sin \phi (\ell \dot{\phi} \cos \phi + \ddot{\lambda} \sin \phi) \\ (e^2 N \cos^2 \phi + \frac{Nb^2}{a^2} + h) \ddot{\phi} \\ e^2 N \ddot{\phi} \cos \phi \sin \phi \end{bmatrix} \quad (3-26)$$

and the centripetal acceleration term of equation (3-9) for the Local Level system is

$$\vec{\omega}_{LL} \times \vec{\omega}_{LL} \times \vec{r}_{LL} = \begin{bmatrix} -l\dot{\phi} \sin \phi \left(\frac{Nb^2}{2} + h \right) \\ e^2 N \dot{\phi}^2 \cos \phi \sin \phi + (N+h)l^2 \cos \phi \sin \phi \\ -\dot{\phi}^2 \left(e^2 N \cos^2 \phi + \frac{Nb^2}{2} + h \right) - (N+h)l^2 \cos^2 \phi \end{bmatrix} \quad (3-27)$$

Substituting equations (3-22), (3-24) (3-26) and (3-27) into (3-9) yields the final expression for the absolute acceleration in the Local Level system as

$$\vec{a}_{LL} = \begin{bmatrix} 2l\dot{h} \cos \phi - 2h\dot{\phi}l \sin \phi - \frac{2(1-e^2)N\dot{\phi}l}{Q^2} \sin \phi + \ddot{\lambda}(N+h) \cos \phi \\ 2\ddot{\phi}h + (N+h)l^2 \sin \phi \cos \phi + \left[\frac{(1-e^2)N}{Q^2} + h \right] \ddot{\phi} + \frac{3(1-e^2)e^2 N \dot{\phi}^2 \sin 2\phi}{2Q^4} \\ \ddot{h} - (N+h)l^2 \cos^2 \phi - \left[\frac{(1-e^2)N}{Q^2} + h \right] \dot{\phi}^2 \end{bmatrix} \quad (3-28)$$

Before obtaining an expression for the specific force, \vec{f}_{LL} , the gravitational attraction of the earth G_{LL} , must be added to the absolute acceleration \vec{a}_{LL} . The gravitation vector along the Local Level axes is obtained by using the normal gravity γ (equation (2-15)) and eliminating the centrifugal force to yield

$$\vec{G}_{LL} = \begin{bmatrix} 0 \\ -\omega_S^2 (N+h) \cos \phi \sin \phi \\ \gamma + \omega_S^2 (N+h) \cos^2 \phi \end{bmatrix} \quad (3-29)$$

Combining equation (3-29) with (3-28) and realizing that

$$M = \frac{(1 - e^2)N}{Q^2} \quad (3-30)$$

yields the specific force equation

$$\vec{f}_{LL} = \begin{bmatrix} 2\ell\ddot{h} \cos \phi - 2h\dot{\ell}\dot{\phi} \sin \phi - 2M\dot{\phi}\dot{\ell} \sin \phi + (N+h)\ddot{\lambda} \cos \phi \\ 2\dot{\phi}\ddot{h} + (N+h)\dot{\lambda}(2\omega_S + \dot{\lambda}) \sin \phi \cos \phi + (M+h)\ddot{\phi} + \frac{3e^2 M \dot{\phi}^2}{2Q^2} \sin 2\phi \\ \ddot{h} - (N+h)\dot{\lambda}(2\omega_S + \dot{\lambda}) \cos^2 \phi - (M+h)\dot{\phi}^2 + \gamma \end{bmatrix} \quad (3-31)$$

The above equation is simplified by using the following equalities, namely

$$\dot{\phi} = \dot{Y}_{LL} / (M + h) \quad , \quad (3-32)$$

$$\dot{\lambda} = \dot{X}_{LL} / ((N + h) \cos \phi) \quad , \quad (3-33)$$

$$\dot{h} = \dot{Z}_{LL} \quad , \quad (3-34)$$

$$\begin{aligned} \ddot{\phi} &= \ddot{Y}_{LL} / (M+h) - 3e^2 M \dot{\phi} \ddot{Y}_{LL} \sin 2\phi / (2(M+h)^2) \\ &= \ddot{Y}_{LL} \dot{Z}_{LL} / (M+h)^2 \quad , \end{aligned} \quad (3-35)$$

and

$$\begin{aligned} \ddot{\lambda} &= \ddot{X}_{LL} / ((N+h) \cos \phi) + \dot{X}_{LL} \dot{Y}_{LL} \sin \phi / [(N+h)(M+h) \cos^2 \phi] \\ &= e^2 N \dot{X}_{LL} \dot{Y}_{LL} \sin \phi / [(N+h)^2 (M+h) Q^2] \\ &= \dot{X}_{LL} \dot{Z}_{LL} / ((N+h)^2 \cos \phi) \quad , \end{aligned} \quad (3-36)$$

which when substituted into equation (3-31) yields the final system of equations

$$\vec{f}_{LL} = \begin{bmatrix} \ddot{X}_{LL} + (2\omega_S + \dot{\lambda})\dot{Z}_{LL} \cos \phi - (2\omega_S + \dot{\lambda})\dot{Y}_{LL} \sin \phi \\ \ddot{Y}_{LL} + \dot{\phi}\dot{Z}_{LL} + (2\omega_S + \dot{\lambda})\dot{X}_{LL} \sin \phi \\ \ddot{Z}_{LL} - \dot{\phi}\dot{Y}_{LL} - (2\omega_S + \dot{\lambda})\dot{X}_{LL} \cos \phi + \gamma \end{bmatrix} \quad (3-37)$$

Similar results may be found in Britting [1971] and Macomber [1966] with slightly different axes orientation and rotation matrix conventions.

3.4 Mechanization of Local Level System

Using the final specific force equation (3-37), one is now capable of solving the positioning problem by double integration of the accelerations in the Local Level frame (\ddot{X}_{LL} , \ddot{Y}_{LL} and \ddot{Z}_{LL}). First, to obtain an overall appreciation of the mechanization process consider Figure 3-2.

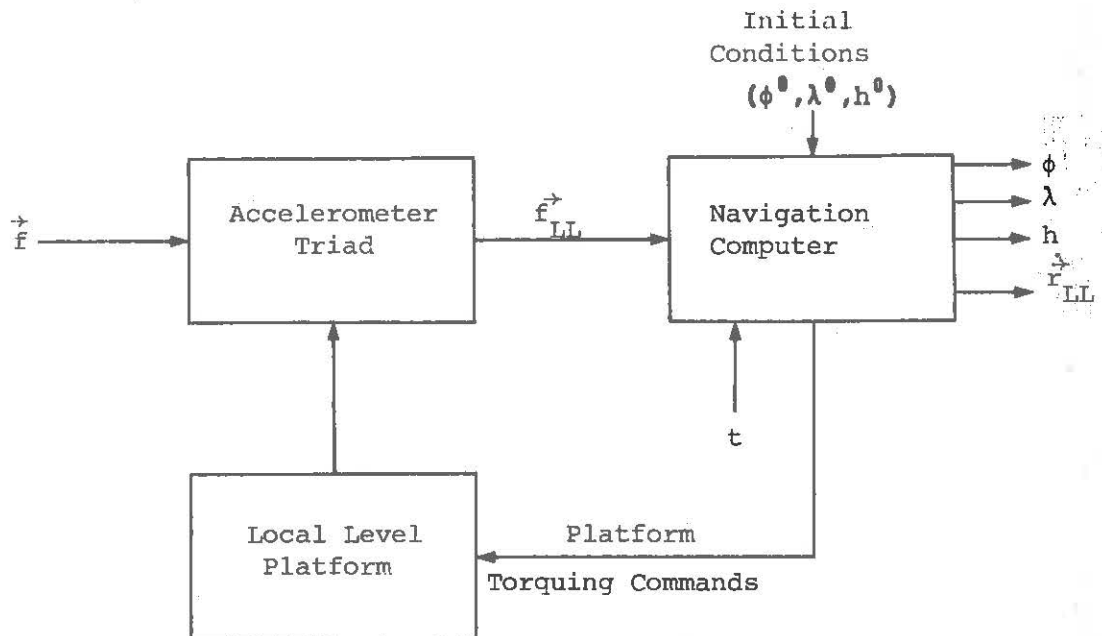


Figure 3-2
Mechanization Overview

The navigation computer receives the specific force measurements from the accelerometers which are in the Local Level frame and then using equation (3-37) it computes the position and torquing commands that must be sent to the gyros and hence to the platform. The application of equation (3-37) is done at discrete time intervals of about 20 milliseconds, and the process is often called the cross product loop.

The details of the mechanization are given in Figure 3-3. It should first be noted that the mechanization process is manufacturer dependent and only the principal points are stressed in this report. The mechanization flowchart, Figure 3-3, is divided into four basic units. The first unit contains the sensors located on the platform. The second unit is the interface between the platform sensors and the navigation computer. The interface shows that the acceleration signal (specific force) is integrated before it reaches the navigation computer. This is a result of an analogue integration circuit that operates on the current output from the accelerometer. Various schemes have been developed for the integration of this output and the manner in which the pulsed output is sent to the navigation computer. The most critical thing to note is the resolution of the pulsed signal sent to the computer. The interface also includes the return signal to the gyro torquers which keep the platform oriented in the Local Level frame. With the return gyro torquer signal the main point of concern is the smallest torque increment possible as this is the limiting accuracy of the orientation error. The sequence of servicing both the accelerometer outputs, and the gyro torquer signals, and the time taken for the servicing are also important considerations.

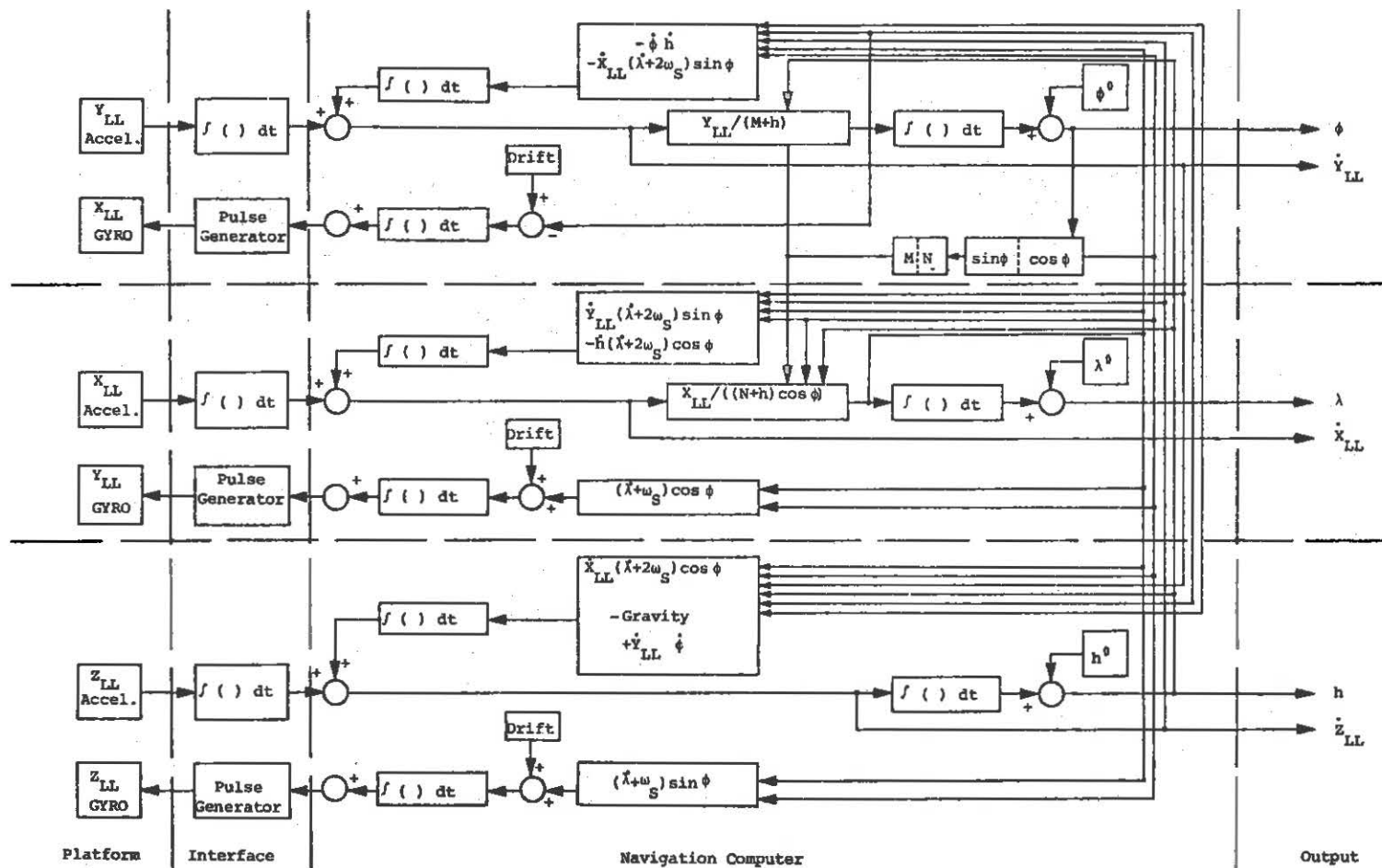


Figure 3-3
Local Level Mechanization

The third unit contains the navigation computer which mechanizes the specific force equation (3-37). This unit may or may not house the Kalman filtering mechanization to be described in Section 4. This is totally dependent on the amount of interaction desired between the filter and the mechanization depicted in Figure 3-3. For the Kalman filter described in this report there is no interaction and the Kalman filter can be housed in a fifth unit which requires only the output as shown in Figure 3-3. Returning to the third unit, navigation computer, it can be seen that this unit mechanizes the cross product loop previously mentioned. Here it is seen that the observed accelerations cannot be directly corrected because the specific force has been integrated. Thus, the cross product terms must be integrated to yield velocity cross product corrections. The application of the cross product corrections are one iteration behind the observed specific force accelerations to which the cross products should be applied. The assumption is that the speed of computations, approximately 40 times per second, takes care of the lag problem. The most critical lag problem is associated with the torquing of the gyros because the computed angular velocity is always one iteration behind the measured accelerations. It is this gyro torquing lag that causes the position error in the simulation results of Section 5, when no errors are introduced. Another lag problem arises from the fact that certain terms are applied in quantum steps with the residual being left to accumulate up to the step value before a pulse may be generated. The same quantum step problem may be observed wherever a summation symbol, indicated by a circle, appears in the navigation computer unit, Figure 3-3. The advent of fast compact digital computers should

virtually eliminate the quantum step problems within the navigation computer.

The output of the system consists of the position as well as the Local Level velocities. There are various other quantities that may be examined by searching through the registers of the computer but they will not be discussed here. The position is the fundamental unknown but the Local Level velocities play a significant part in the coordinate smoothing procedures to be described in the subsequent sections on zero velocity updating and Kalman filtering.

3.5 Platform Alignment

Before one is able to implement the Local Level mechanization as described in Section 3-3, the platform and its sensors must physically instrument the Local Level frame. The process of platform alignment is of importance because it is this process which will introduce errors in the initial orientation. To explain the principle, one of the various methods of platform alignment is described here. The simulation to be subsequently presented assumes perfect initial alignment because very little is known of the exact techniques used in inertial surveying systems.

The process of alignment described here involves an accelerometer/gyro servo loop. The method begins by monitoring the accelerometer outputs in the X_{LL} and Y_{LL} channels (east and north channels respectively). The gyros may then be torqued until no component of acceleration is sensed in either channel (levelling of platform). This, from equation (3-37), means that the X_{LL}, Y_{LL} plane is normal to the local gravity vector. The Y_{LL} axis may not be pointing north

however, and the angular velocity of the platform compensation for the earth rate, equation (3-18), will introduce a measurable angular velocity about the X_{LL} axis at a rate [Britting, 1971] of $\Delta AZ \omega_S \cos \phi$, where ΔAZ is the azimuth misalignment. This will eventually introduce an acceleration to the Y_{LL} channel accelerometer. This acceleration is driven to zero by torquing the azimuth gyro until this acceleration is eliminated (gyrocompassing). The levelling and gyrocompassing are performed simultaneously and at very fast rates. More details on alignment procedures are given in, for example, Farrell [1976] or Britting [1971].

It should be noted that the Local Astronomic [Krakiwsky and Wells, 1971] and not the Local Level frame is instrumented in actual application. However, as previously mentioned, a normal gravity field is assumed throughout this report and the difference between the two frames does therefore not materialize.

3.6 Zero Velocity Update

The zero velocity update (ZUPT) is a procedure used to reduce the position error by means of monitoring velocity output when the inertial system is stationary. In this section the basic procedure as well as a simple update algorithm will be discussed. The subsequent section on Kalman filtering will present a more sophisticated, though not entirely rigorous, approach to velocity updating.

While the inertial platform is stationary the velocity outputs, Figure 3-3, should be zero. Assuming that at the initial point the alignment of the platform with the local gravity vector and the instantaneous rotation axis was done correctly, the velocity output

at that time in all three channels would be zero (i.e. all cross products perfectly compensated). After navigating from the initial point to a second point, the platform will be slightly out of alignment because of drifts and biases in the components, random errors in the measurements and anomalous gravity field components. Because the platform is out of alignment there will be accelerations detected and therefore velocities computed. These velocities, in addition to the residual velocities from the computational algorithm used during the traverse period, are monitored during the ZUPT, and then corrections are applied to the current coordinates based on some model for the velocity error/time curve. A simple model for coordinate corrections is to assume that the velocity error/time curve is a linear one in each channel. For example, consider the hypothetical velocity error/time curve for a chosen channel depicted in Figure 3-4.

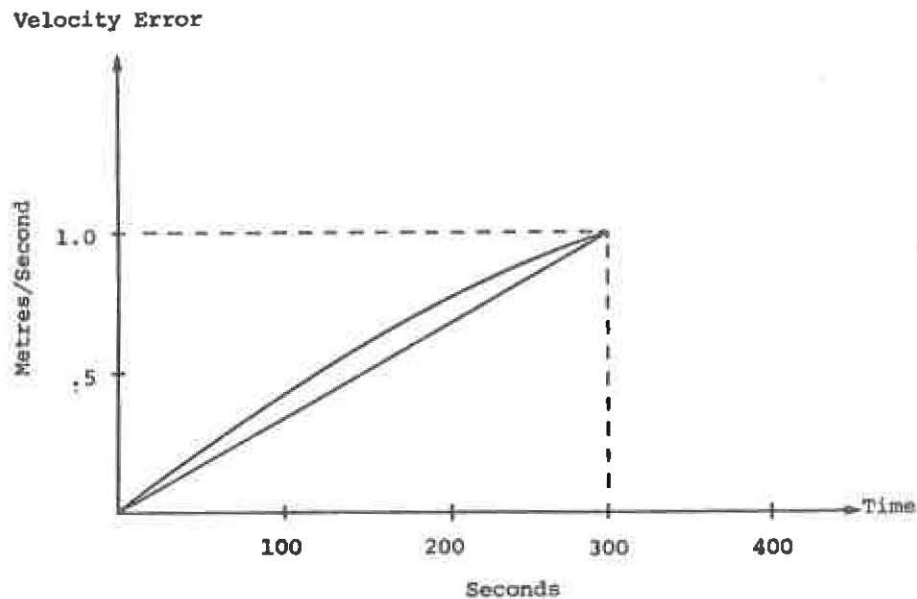


Figure 3-4

Velocity Error / Time Curve

The curved line represents the actual velocity error curve and the area under this curve would be the correction to be applied to the position at the 300 second point. If the assumption that the velocity error/time curve was a straight line is used, then the correction to the position would be the triangle area, namely

$$\Delta \text{ POSITION} = \Delta t \cdot \Delta V / 2 \quad , \quad (3-38)$$

where $\Delta \text{ POSITION}$ is the correction to the coordinate, Δt is the elapsed time since all channels had zero velocity, and ΔV is the velocity error at the time of the update.

For the Local Level system the geodetic ellipsoidal quantities of latitude, longitude, and height are the output coordinates. This immediately implies using the velocities in these terms, namely

$$\dot{\phi} = \dot{Y}_{LL} / (M + h) \quad (3-39)$$

= latitude velocity ,

$$\dot{\lambda} = \dot{X}_{LL} / ((N + h) \cos \phi) \quad (3-40)$$

= longitude velocity ,

and

$$\dot{h} = \dot{Z}_{LL} \quad (3-41)$$

= height velocity ,

for position corrections at a ZUPT.

The correction to the output coordinates at a zero velocity update could then be written, using equations (3-39) to (3-41) as

$$\phi_{\text{CORR}} = \phi - \Delta t \Delta \dot{\phi} / 2 \quad (3-42)$$

$$\lambda_{\text{CORR}} = \lambda - \Delta t \Delta \dot{\lambda} / 2 \quad (3-43)$$

and

$$h_{\text{CORR}} = h - \Delta t \Delta \dot{h} / 2 \quad (3-44)$$

The velocities in the above equations are the velocities obtained while the vehicle is stationary.

Besides the correction of the position there are a few other options available during a ZUPT. The first option is whether or not to zero all the velocity stores before continuing on to the next traverse leg. The zero velocity update procedure described in this section requires that the stores be zeroed, or the unbounded height velocity errors will eventually cause large position errors in all channels (see Section 5). The second option is whether or not to realign the platform at a zero velocity update. For the simple ZUPT of this section no information is directly provided which estimates the misorientation of the system and therefore a complete realignment as described in Section 3.4 would be required. To eliminate this, no realignment is performed for the simulation results using the simple ZUPT in Section 5.

4. KALMAN FILTERING

The objective of this section is to present the general concepts of Kalman filtering and then show a particular application of the technique for the Local Level inertial survey system.

4.1 Kalman Filtering Concepts

The Kalman filtering technique is used primarily for dynamic systems where real time estimates of unknowns and their associated covariance matrices are required. A summary of the filtering expressions may be found in Kalman [1960] or Krakiwsky [1975]. Using the notation adopted by Krakiwsky [1975], with the Σ symbol replaced by C , a brief description of the Kalman expressions is presented here.

The basic equation involves the prediction of the state as

$$\hat{X}'_{i+1} = \Phi X'_i, \quad (4-1)$$

uxl uxu ux1

where \hat{X}'_i and \hat{X}'_{i+1} are the random variable state vectors at time $t = i$, and time $t = i + 1$ respectively. The state vector contains the random variables pertaining to the parameters being solved for. The prime symbol, $()'$, is used to indicate that the quantity is

predicted. The symbol \hat{X} is best explained by writing

$$\hat{X} = X - \hat{X} \quad , \quad (4-2)$$

where \hat{X} is the adjusted state vector, X is the computed value (from mechanization equations) for the state vector, and \hat{X} is the weighted least squares estimate of the correction to the computed state vector. The remaining term of equation (4-1) is the transition matrix Φ , which is representative of the dynamic model being used. It is the formation of an explicit form of the transition matrix that presents the most difficulty in inertial surveying applications. The transition matrix may be defined as the matrix containing in columns the u independent solutions to the system of linear differential equations

$$\begin{matrix} \dot{X} \\ X \end{matrix} = \begin{matrix} A_1 \\ \text{uxl uxu uxl} \end{matrix} \hat{X} \quad , \quad (4-3)$$

under the conditions

$$\Phi(t^0) = I \quad , \quad (4-4)$$

and

$$\begin{matrix} \dot{\Phi} \\ \Phi \end{matrix} = \begin{matrix} A_1 \\ \text{uxu uxu uxu} \end{matrix} \Phi \quad , \quad (4-5)$$

where the symbol $\dot{(\)}$ denotes time derivative and the symbol $(\)^0$ denotes initial value. The difference between the fundamental matrix [Boyce and DiPrima, 1969] and the transition matrix defined above is

that the initial condition equation (4-4) is not normalized for the fundamental matrix. The matrix A_1 in equations (4-3) and (4-5) is the matrix of coefficients that describes the relationship between the state vector corrections.

The next expression that is considered is that for the prediction of the covariance matrix of the state vector, namely [Krakiwsky, 1975]

$$\hat{C}_{X_{i+1}}^{uxu} = \sigma_0^2 [\Phi(N_i + P_X)^{-1} \Phi^T + P_m^{-1}] \quad (4-6)$$

The σ_0^2 is the a priori variance factor and for the purposes of this study will be considered known and equal to 1. N_i can be considered as the inverse of the predicted covariance matrix at time $t = i$, namely

$$N_i = (C_{X_i}^{\hat{}})^{-1} \quad (4-7)$$

The P_X matrix is the inverse of the covariance matrix of the initial conditions and is considered only on the first application of equation (4-6). An expression for the P_X matrix may be given as

$$P_X = (C_{X^0})^{-1} \quad (4-8)$$

where X^0 refers to the initial state vector. The P_m^{-1} term in equation (4-6) is the covariance matrix of the model errors and it reflects the uncertainties in the mathematical model and the mechanical

components.

In practice equation (4-1) and the condensed form of equation (4-6)

$$\hat{X}_{i+1} = [\Phi \hat{C}_{X_i}^T \Phi^T + P_m^{-1}] \quad (4-9)$$

must be repeated many times before external information is provided that enables the updating of the state vector and its covariance matrix. When additional information is provided the next step in the Kalman filter process is the computation of the gain matrix by [Krakiwsky, 1975]

$$G = \hat{C}_{X_j}^T A_2^T [M_2 + A_2 \hat{C}_{X_j}^T A_2^T]^{-1} \quad (4-10)$$

where r is the number of observation equations of the form

$$F(\bar{X}, \bar{L}) = 0 \quad (4-11)$$

where the symbol $(\bar{\quad})$ indicates an error free quantity and L is the vector of n observations. The matrix A_2 is a design matrix given by

$$A_2 = \frac{\partial F(X, L)}{\partial X} \quad (4-12)$$

The M_2 matrix is given by

$$M_2 = \begin{matrix} B & C_L & B^T \\ \text{rxn} & \text{nxn} & \text{nxr} \end{matrix} , \quad (4-13)$$

where C_L the covariance matrix of the observations and the design matrix B is given by

$$B = \frac{\partial F(X, L)}{\partial L} . \quad (4-14)$$

The C_{X_j} is the last predicted covariance matrix computed before the additional observations were provided.

After the computation of the gain matrix the next step involves the computation of the estimated correction to the state vector by [Krakiwsky, 1975]

$$\hat{X}_j = \hat{X}'_j - G(W + A_2 \hat{X}'_j) , \quad (4-15)$$

rxl

where the W vector is the vector of misclosures given by

$$W = F(X, L) . \quad (4-16)$$

Having obtained the estimated correction to the state vector the corrected estimate of the state vector from equation (4-2) is given by

$$\hat{X}_j = X_j - \hat{X}_j . \quad (4-17)$$

The last term to be computed is the covariance matrix of the estimated state vector [Krakiwsky, 1975]

$$\hat{C}_{X_j} = [\hat{C}_{X_j} - G A_2 \hat{C}_{X_j}] \quad (4-18)$$

This covariance matrix completes the description of the Kalman expressions.

4.2 Kalman Filtering Expressions for Local Level Mechanization

Having described the basic filter equations the next objective is to implement these equations for a special case of the Local Level inertial navigation process as described in Britting [1971]. The special case considered is that in which the state vector is given by

$$\hat{X}^T = [\hat{\Psi}_{Y_{LL}}, \hat{\Psi}_{X_{LL}}, \hat{\Psi}_{Z_{LL}}, \hat{\phi}, \hat{\lambda}, \dot{\hat{\phi}}, \dot{\hat{\lambda}}] \quad (4-19)$$

where $\hat{\Psi}$ is the misorientation about the designated axis, $\hat{\phi}$ and $\hat{\lambda}$ are the latitude and longitude corrections and $\dot{\hat{\phi}}$ and $\dot{\hat{\lambda}}$ are the latitude and longitude velocity corrections. It is immediately evident that the height and height velocity terms have been neglected from this development which gives the same effect as eliminating the vertical accelerometer. For a more rigorous development the vertical channel must be included.

Using the specified state vector, equation (4-19), the system of linear differential equations, equation (4-3), must now be constructed. The first three rows of the design matrix A_1 pertain to the misorientation unknowns. To deal with these rows first consider the

expression

$$\dot{\vec{\Psi}} = \vec{e}_{\omega} + \hat{\vec{\omega}}_{LL} - \vec{\omega}_{LL} \times \vec{\Psi} \quad (4-20)$$

where \vec{e}_{ω} is the random component of the misorientation drift and $\hat{\vec{\omega}}_{LL}$ is the navigation mechanization feed back error. Expanding $\hat{\vec{\omega}}_{LL}$ yields

$$\hat{\vec{\omega}}_{LL} = \vec{\omega}_{LL}^{AC} - \vec{\omega}_{LL} \quad (4-21)$$

where $\vec{\omega}_{LL}$ is given by equation (2-15) and represents the desired or ideal commanded angular velocity and $\vec{\omega}_{LL}^{AC}$ is the actual commanded angular velocity. To obtain the contribution of the elements of the state vector to equation (4-20) the total derivative of (4-21) is taken to yield

$$\hat{\vec{\omega}}_{LL} = \frac{\partial \vec{\omega}_{LL}}{\partial \mathbf{X}} \hat{\mathbf{X}} \quad (4-22)$$

The final term in equation (4-20), $-\vec{\omega}_{LL} \times \vec{\Psi}$, is responsible for indicating how a misorientation error propagates with applied angular velocity. The negative sign insures that the contribution of the term is compatible with the $\hat{\vec{\omega}}_{LL}$ term. The final differential equation for the misorientation elements is then written as

$$\dot{\vec{\Psi}} = \frac{\partial \vec{\omega}_{LL}}{\partial \mathbf{X}} \hat{\mathbf{X}} - \vec{\omega}_{LL} \times \vec{\Psi} + \vec{e}_{\omega} \quad (4-23)$$

To arrive at the elements of the A matrix given in Britting [1971, pg. 230] the commanded angular velocity about the Y_{LL} , X_{LL} and $-Z_{LL}$ axes (north, east and down axes) is rewritten as

$$\vec{\omega}_{LL} = \begin{bmatrix} (\omega_S + \dot{\lambda}) \cos \phi \\ -\dot{\phi} \\ -(\omega_S + \dot{\lambda}) \sin \phi \end{bmatrix}, \quad (4-24)$$

before computing (4-23). The change of order in the expression (4-24) is done to make it compatible with the order of the orientation terms in the state vector. Evaluating the second term of equation (4-23) yields

$$-\vec{\omega}_{LL} \times \hat{\Psi} = \begin{bmatrix} \dot{\phi} \hat{\Psi}_{Z_{LL}} - (\omega_S + \dot{\lambda}) \hat{\Psi}_{X_{LL}} \sin \phi \\ (\omega_S + \dot{\lambda}) \hat{\Psi}_{Z_{LL}} \cos \phi + (\omega_S + \dot{\lambda}) \hat{\Psi}_{Y_{LL}} \sin \phi \\ -\dot{\phi} \hat{\Psi}_{Y_{LL}} - (\omega_S + \dot{\lambda}) \hat{\Psi}_{X_{LL}} \cos \phi \end{bmatrix}, \quad (4-25)$$

while equation (4-22) yields

$$\frac{\partial \vec{\omega}_{LL}}{\partial X} \hat{X} = \begin{bmatrix} \dot{\lambda} \cos \phi - (\omega_S + \dot{\lambda}) \dot{\phi} \sin \phi \\ -\dot{\phi} \\ -\dot{\lambda} \sin \phi - (\omega_S + \dot{\lambda}) \dot{\phi} \cos \phi \end{bmatrix} \quad (4-26)$$

The final terms of the design matrix A_1 are found by combining (4-26) and (4-25) with (4-23) to yield

$$A_1(1, 2) = -(\omega_S + \dot{\lambda}) \sin \phi \quad , \quad (4-27)$$

$$A_1(1, 4) = -(\omega_S + \dot{\lambda}) \sin \phi \quad , \quad (4-28)$$

and

$$A_1(1, 7) = \cos \phi \quad , \quad (4-29)$$

where the $\dot{\phi} \Psi_{Z_{LL}}$ term is omitted as it is of a much smaller magnitude than the other terms. The second row of the design matrix has the elements

$$A_1(2, 1) = (\omega_S + \dot{\lambda}) \sin \phi \quad , \quad (4-30)$$

$$A_1(2, 3) = (\omega_S + \dot{\lambda}) \cos \phi \quad , \quad (4-31)$$

and

$$A_1(2, 6) = -1 \quad , \quad (4-32)$$

The third row is given by

$$A_1(3, 2) = -(\omega_S + \dot{\lambda}) \cos \phi \quad , \quad (4-33)$$

$$A_1(3, 4) = -(\omega_S + \dot{\lambda}) \cos \phi \quad , \quad (4-34)$$

and

$$A_1(3, 7) = -\sin \phi \quad , \quad (4-35)$$

where the $-\dot{\phi} \hat{\Psi}_{Y_{LL}}$ is omitted because it is of a much smaller magnitude than the other terms.

Turning to the ellipsoidal coordinate elements of the state vector, the differential expressions may be written immediately as

$$\dot{\hat{\phi}} = \dot{\phi} \quad (4-36)$$

and

$$\dot{\hat{\lambda}} = \dot{\lambda} \quad (4-37)$$

which accounts for the elements in the fourth and fifth rows of the design matrix A_1 .

The single element pertaining to the latitude velocity may be obtained by knowing that the contribution to the latitude velocity from a misorientation about the X_{LL} axis is given approximately as

$$\ddot{\hat{\phi}} = (\gamma/R) \hat{\Psi}_{X_{LL}} \quad (4-38)$$

where γ is the normal gravity and the radius term is given by

$$R = \sqrt{MN} \quad (4-39)$$

The terms involving the latitude, latitude velocity, longitude velocity, and $\hat{\Psi}_{Z_{LL}}$ misorientation have all been neglected when computing the row of the differential equation pertaining to the latitude velocity.

The only element of the row pertaining to the longitude velocity, $\dot{\hat{\lambda}}$, is given by the misorientation about the Y_{LL} axis, namely

$$\ddot{\hat{\lambda}} = \frac{-\dot{\gamma}}{R \cos \phi} \hat{\Psi}_{Y_{LL}} \quad (4-40)$$

where the same terms neglected when dealing with the latitude velocity are neglected here as well.

The final form of the A_1 design matrix using the above information is

$$A_1 = \begin{bmatrix} 0 & -\ell \sin \phi & 0 & -\ell \sin \phi & 0 & 0 & \cos \phi \\ \ell \sin \phi & 0 & \ell \cos \phi & 0 & 0 & -1 & 0 \\ 0 & -\ell \cos \phi & 0 & -\ell \cos \phi & 0 & 0 & \sin \phi \\ 0 & 0 & 0 & 0 & 0 & 1 & 0 \\ 0 & 0 & 0 & 0 & 0 & 0 & 1 \\ 0 & \gamma/R & 0 & 0 & 0 & 0 & 0 \\ -\gamma/(R \cos \phi) & 0 & 0 & 0 & 0 & 0 & 0 \end{bmatrix} \quad (4-41)$$

where $\ell = \omega_S + \dot{\lambda}$. The above expression is identical to that given in Britting [1971].

The next problem is to find the transition matrix for the system of differential equations (4-3) subject to the initial condition equation (4-4). Boyce and DiPrima [1969] use the Laplace transform techniques as one approach to solving the problem, and that is what is utilized here. There are other methods [Liebelt, 1967] but most are not suited for obtaining the explicit form of the transition matrix for successive applications of the Kalman filtering equations. The advent of mini computers may possibly result in the use of numerical

algorithms for solving the system of differential equations. The problem will most likely be a question of time, i.e., is one able to compute an updated transition matrix for every application of the Kalman prediction equations (4-1) and (4-9)?

Returning to the Laplace transform techniques, the expression for the transition matrix may be written as [Boyce and DiPrima, 1969; Britting, 1971]

$$\Phi(t) = L_T^{-1} [(sI - A_1)^{-1}] \quad , \quad (4-42)$$

where L_T^{-1} denotes the inverse Laplace transform. The use of the inverse Laplace transform may yield different forms for the transition matrix elements depending on the type of factoring used in computing the elements but the final results are numerically equivalent. The objective is to solve equation (4-3) with A_1 given by (4-41) in such a way that the approximations made in Britting [1971, pg. 231] become evident.

Applying (4-42) to (4-41) results in

$$\Phi(t) = L_T^{-1} \left[\begin{array}{ccc|ccc} s & l \sin \phi & 0 & l \sin \phi & 0 & 0 & -\cos \phi \\ -l \sin \phi & s & -l \cos \phi & 0 & 0 & 1 & 0 \\ 0 & l \cos \phi & s & l \cos \phi & 0 & 0 & -\sin \phi \\ \hline 0 & 0 & 0 & s & 0 & -1 & 0 \\ 0 & 0 & 0 & 0 & s & 0 & -1 \\ 0 & -\gamma/R & 0 & 0 & 0 & s & 0 \\ \gamma/(R \cos \phi) & 0 & 0 & 0 & 0 & 0 & s \end{array} \right]^{-1} \quad (4-43)$$

Taking the inverse of the above matrix is the most difficult task. For this particular application the matrix partitioning methods described by Faddeev and Faddeeva [1963] are well suited. To summarize the method a matrix J is partitioned as follows

$$J = \begin{bmatrix} A & | & B \\ \hline C & | & D \end{bmatrix} \quad , \quad (4-44)$$

with the inverse given by

$$J^{-1} = \begin{bmatrix} K & | & L \\ \hline M & | & N \end{bmatrix} \quad , \quad (4-45)$$

where

$$K = (A - BD^{-1}C)^{-1} \quad , \quad (4-46)$$

$$M = -D^{-1}CK \quad , \quad (4-47)$$

$$L = KBD^{-1} \quad , \quad (4-48)$$

and

$$N = D^{-1} - D^{-1}CL \quad , \quad (4-49)$$

Returning to (4-43) the partitioning is done as indicated by the dotted lines. The matrix D^{-1} may be easily derived using standard cofactor techniques to yield

$$D^{-1} = \begin{bmatrix} 1/s & 0 & 1/s^2 & 0 \\ 0 & 1/s & 0 & 1/s^2 \\ 0 & 0 & 1/s & 0 \\ 0 & 0 & 0 & 1/s \end{bmatrix} \quad , \quad (4-50)$$

Performing the multiplication of equation (4-46) and evaluating the determinant yields

$$\begin{aligned} \text{DET} &= |A - BD^{-1}C| \\ &= (s + \gamma/(sR))^2 (s + \ell^2/s) \end{aligned} \quad (4-51)$$

and the transposed cofactor matrix for $(A - BD^{-1}C)$ is given by

$$\begin{bmatrix} s(s+\gamma/(sR)) & -s\ell \sin \phi(1+ & -\ell^2 \sin \phi \cos \phi(1 \\ +\ell^2(1+\gamma/(s^2R)) \cos^2 \phi & \gamma/(s^2R)) & +\gamma/(s^2R)) \\ \\ \ell s \sin \phi & s(s+\gamma/(sR)) & (s+\gamma/(sR))\ell \cos \phi \\ +\ell \gamma \sin \phi/(sR) & & \\ \\ \ell \sin \phi(\ell \cos \phi & -(s+\gamma/(sR))(1 & (s+\gamma/(sR))^2 \\ +\ell \gamma \cos \phi/(s^2R)) & +\gamma/(s^2R))\ell \cos \phi & +\ell \sin^2 \phi(1+ \\ +(s+\gamma/(sR))(\gamma & -\gamma\ell(1+\gamma/(s^2R)) & \gamma/(s^2R)) \\ \tan \phi/(sR)) & \tan \phi \sin \phi/(sR) & \end{bmatrix} \quad (4-52)$$

From (4-52), in combination with (4-51), the inverse Laplace transforms may be taken to yield the elements in the top left hand corner (3 x 3) of the transition matrix. A few elements are derived here to show the procedure and the typical approximations made. The (1, 1) element of the transition matrix is given by

$$\phi(1,1) = L_T^{-1} \left[\frac{s(s+\gamma/(sR)) + \ell^2(1+\gamma/(s^2R)) \cos^2 \phi}{\text{DET}} \right] \quad (4-53)$$

Britting [1971] makes the simplifying assumption that the first term is much greater than the second term and also that

$$\frac{\ell^2}{s} \approx 0 \quad (4-54)$$

which reduces (4-53) to

$$\begin{aligned} \phi(1,1) &= L_T^{-1} [s/(s^2 + \gamma/R)] \\ &= \cos(t\sqrt{\gamma/R}) \end{aligned} \quad (4-55)$$

The $\phi(2,2)$ element will be identical using the (4-54) approximation.

Before stating the full transition matrix a more involved term is treated. Consider the $\phi(2,1)$ element given by

$$\phi(2,1) = L_T^{-1} \left[\frac{s\ell \sin \phi + \ell\gamma \sin \phi / (sR)}{\text{DET}} \right] \quad (4-56)$$

which when factored yields

$$\phi(2,1) = L_T^{-1} \left[\frac{\ell s^2 \sin \phi}{(s^2 + \gamma/R)(s^2 + \ell^2)} \right] \quad (4-57)$$

Using the convolution theorem for the Laplace transforms [Abramowitz and Stegun, 1972]

$$L_T^{-1} (f_1(s)f_2(s)) = \int_0^t F_1(t - \tau)F_2(\tau) d\tau \quad (4-58)$$

equation (4-57) may be reduced to

$$\begin{aligned} \phi(2,1) = \ell \sin \phi & \left[\frac{\sin(t\sqrt{\gamma/R})}{2(\sqrt{\gamma/R} - \ell)} + \frac{\sin(t\sqrt{\gamma/R})}{2(\sqrt{\gamma/R} + \ell)} \right. \\ & \left. - \frac{\sin(\ell t)}{2(\sqrt{\gamma/R} - \ell)} + \frac{\sin(\ell t)}{2(\sqrt{\gamma/R} + \ell)} \right] \end{aligned} \quad (4-59)$$

and then using the assumption that

$$\sqrt{\gamma/R} \gg \ell \quad (4-60)$$

(4-59) may be rewritten as

$$\phi(2,1) = \frac{\ell \sin \phi}{\sqrt{\gamma/R}} \left[\sin(t\sqrt{\gamma/R}) - \frac{\sin(\ell t)}{\sqrt{\gamma/R}} \right] \quad (4-61)$$

which is the final desired expression. The above examples demonstrate the order of approximations made and the typical procedure for computing the transition matrix. The transition matrix formed in the above fashion for the system of differential equations (4-3) is given in Figure 4-1 where the Schuler frequency $\sqrt{\gamma/R}$ has been denoted by

$$\sqrt{\gamma/R} = \mu \quad (4-62)$$

The next matrices that must be described are those used in equation (4-6). The covariance matrix C_{X_0} in expression (4-8) has the form (at time $t = 0$)

$$\phi = \begin{bmatrix}
 \cos \mu t & \frac{-l}{\mu} \sin \phi (\sin \mu t) & \frac{l^2}{2\mu^2} \sin 2\phi (\cos \mu t - \cos 2t) & \frac{-l}{\mu} \sin \phi (\sin \mu t) & 0 & 0 & \frac{\cos \phi}{\mu} \sin \mu t \\
 \frac{l}{\mu} \sin \phi (\sin \mu t) & \cos \mu t & \frac{l}{\mu} \cos \phi (\sin \mu t) & \frac{-l^2}{\mu^2} (\cos 2t - \cos \mu t) & 0 & \frac{-1}{\mu} \sin \mu t & 0 \\
 \tan \phi (\cos 2t) & -\sec \phi (\sin 2t) & \cos 2t & -\sec \phi (\sin 2t) & 0 & 0 & \frac{-\sin \phi}{\mu} \sin \mu t \\
 -\cos \mu t) & \frac{-l}{\mu} \sin^2 \phi \sin \mu t) & & \frac{-l}{\mu} \sin^2 \phi \sin \mu t) & & & \\
 \sin \phi (\sin 2t) & \cos 2t - \cos \mu t & \cos \phi (\sin 2t) & \cos 2t & 0 & \frac{1}{\mu} \sin \mu t & 0 \\
 \frac{-l}{\mu} \sin \mu t) & & \frac{-l}{\mu} \sin \mu t) & & & & \\
 \sec \phi (\cos \mu t) & \tan \phi (\sin 2t) & \sin \phi (1 - \cos 2t) & \tan \phi (\sin 2t) & 1 & 0 & \frac{1}{\mu} \sin \mu t \\
 -\cos^2 \phi - \sin^2 \phi) & \frac{-l}{\mu} \sin \mu t) & & \frac{-l}{\mu} \sin \mu t) & & & \\
 \cos 2t) & & & & & & \\
 l \sin \phi (\cos 2t) & \mu \sin \mu t & l \cos \phi (\cos 2t) & -l (\sin 2t) & 0 & \cos \mu t & 0 \\
 -\cos \mu t) & & -\cos \mu t) & \frac{-l}{\mu} \sin \mu t) & & & \\
 -\mu \sec \phi (\sin \mu t) & l \tan \phi (\cos 2t) & l \sin \phi (\sin 2t) & l \tan \phi (\cos 2t) & 0 & 0 & \cos \mu t \\
 \frac{-l}{\mu} \sin^2 \phi \sin 2t) & -\cos \mu t) & \frac{-l}{\mu} \sin \mu t) & -\cos \mu t) & & &
 \end{bmatrix}$$

Figure 4-1
Transition Matrix

$$\sigma_{\psi_{Y_{LL}}}^2 = n \sigma_{\psi_{Y_{LL}}}^2, \quad (4-67)$$

and

$$\sigma_{\psi_{Z_{LL}}}^2 = n \sigma_{\psi_{Z_{LL}}}^2, \quad (4-68)$$

where Δt is the time required for the completion of a cross product loop. The terms $\sigma_{Y_{LL}}^2$ and $\sigma_{X_{LL}}^2$ are the variances on the observed accelerations. The $\sigma_{\psi_{X_{LL}}}^2$, $\sigma_{\psi_{Y_{LL}}}^2$, and $\sigma_{\psi_{Z_{LL}}}^2$ are the variances on the gyro random drift. The above terms are not to be confused with the \hat{C}_X terms of equation (4-63) which apply only at time $t = 0$. The n term in equations (4-64) to (4-69) is the number of cross product loops that have been completed between successive applications of the prediction equations. The final form of the P_m^{-1} matrix is then

$$P_m^{-1} = \begin{bmatrix} \sigma_{\psi_{Y_{LL}}}^2 & & & & & & \\ & \sigma_{\psi_{X_{LL}}}^2 & & & & & \\ & & \sigma_{\psi_{Z_{LL}}}^2 & & & & \\ & & & 0 & & & \\ & & & & 0 & & \\ & & & & & \sigma_{\phi}^2 & \\ & & & & & & \sigma_{\lambda}^2 \end{bmatrix} \quad (4-69)$$

The next matrices that must be defined are those associated with the gain matrix (4-10) which is computed at each ZUPT. The A_2 matrix (4-12) relates the observed velocity errors at a ZUPT to the elements of the state vector (4-19). The misorientation is not observed for purposes of this study and it is assumed that the final point of the traverse is unknown. Under these assumptions the A_2 design matrix is

$$A_2 = \begin{bmatrix} 0 & 0 & 0 & 0 & 0 & 1 & 0 \\ 0 & 0 & 0 & 0 & 0 & 0 & 1 \end{bmatrix} \quad (4-70)$$

The M_2 matrix (4-12) is the covariance matrix of the observations (B_2 is an identity matrix) and is given by

$$C_L = \begin{bmatrix} \sigma_{L\phi}^2 & \\ & \sigma_{L\lambda}^2 \end{bmatrix} \quad (4-71)$$

where

$$\sigma_{L\phi}^2 = \sigma_{\phi}^2 \quad (4-72)$$

and

$$\sigma_{L\lambda}^2 = \sigma_{\lambda}^2 \quad (4-73)$$

The remaining vector that must be defined is the misclosure vector W which from (4-16) is

$$W = \begin{bmatrix} -L_{\phi} \\ \phi \\ -L_{\lambda} \end{bmatrix} \quad (4-74)$$

Numerical results using assumed values for the variances are given in Section 5.3. Because there is no term in the development here to account for the large gyro drifts being used in the simulation program, there are three terms added to the covariance matrix of the state vector at each zero velocity update to account for the increased variance in the misorientation. These terms are added to the variances of the misorientation elements ((1,1), (2,2) and (3,3) positions of equation (4-18)) and are of the form

$$\sigma_D^2 = (\text{DRIFT} \cdot t)^2, \quad (4-75)$$

where DRIFT is the expected magnitude of the gyro drifts, and t is the elapsed time since the last alignment.

The Kalman filter developed in this section is not a rigorous one as can be seen from the approximations noted, but the empirical results appear quite reasonable (Section 5.3) and the basic method of Kalman filtering has been demonstrated. Because the seven elements of the state vector are computed using the two observed velocities, the simulation Kalman filter does not correct the computed position, velocity, and misorientation of each ZUPT, as far as the mechanization itself is concerned. The position is corrected for output only, and the accumulated error is left to propagate through the mechanization equations of Section 3.4. It should be noted that with higher gyro drifts and accelerometer biases the application of equation (4-17) would help bound the effect of the systematic errors by eliminating too much cross product interaction. Before applying equation (4-17) as many observations as possible should be accumulated to justify the application of the correction.

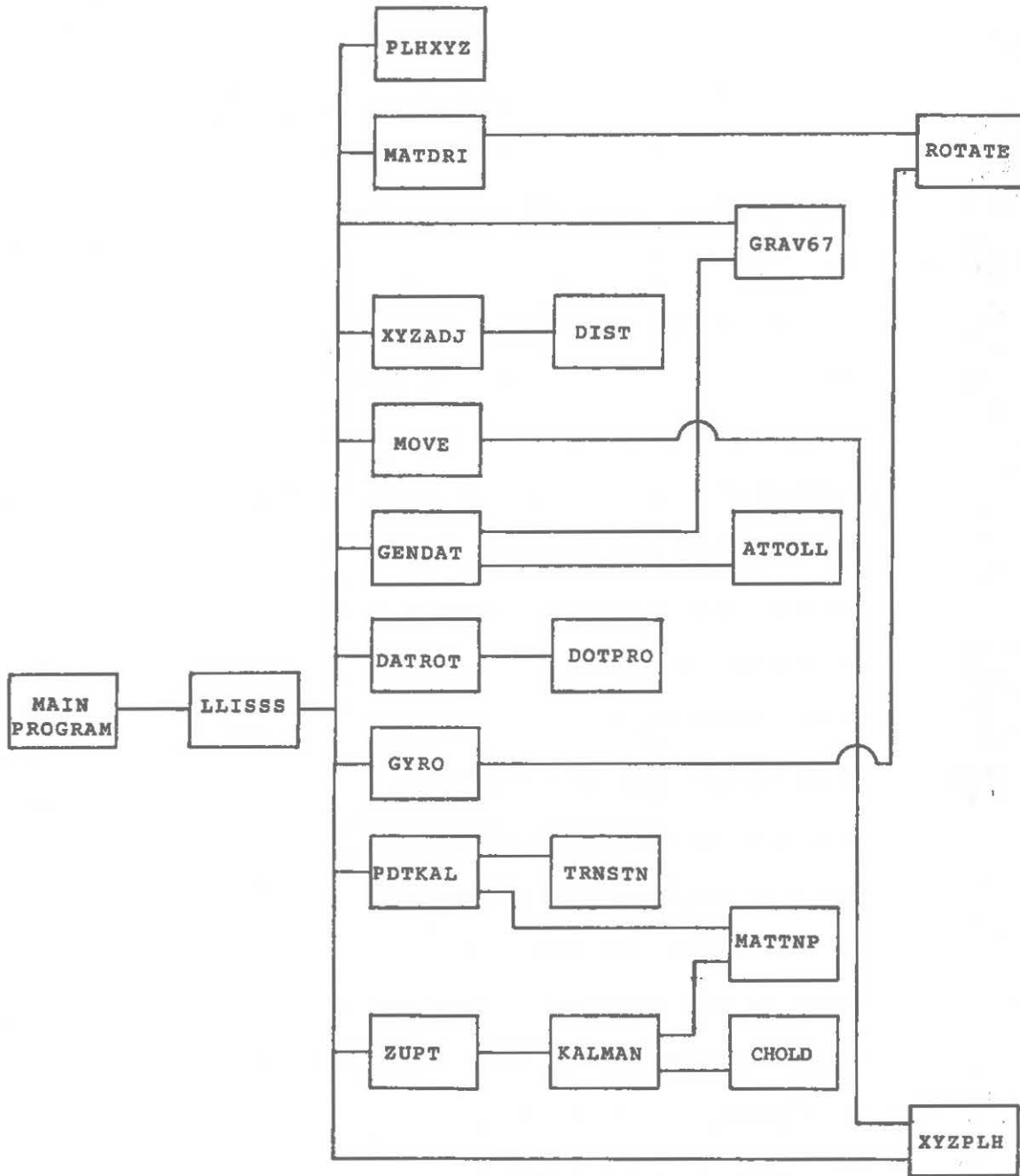
5. LOCAL LEVEL SIMULATION

The purpose of this section is to demonstrate, by means of a Fortran simulation program, the characteristics of the Local Level inertial system. It should be noted that the results stated here only show the capabilities of the simulation program for a few instructive examples. The purpose of the simulation program is to provide useful information for analysing data from an actual system. The program can be further developed to include more rigorous filtering equations and an anomalous gravity field model.

Throughout this study the normal gravity field given by equation (2-16) has been assumed. It has also been assumed that the primary axis of the Earth frame or Instantaneous Terrestrial System is coincident with the semi-minor axis of the chosen reference ellipsoid, and therefore coordinates of the traverse points do not have to be rotated to account for polar motion.

5.1 General Flowchart

The simulation subroutine flowchart is given in Figure 5-1. The flowchart should be read from left to right, top to bottom. A brief description is given as to the contents of each subroutine depicted in Figure 5-1. No attempt is made to give a detailed flowchart because of the length of the simulation program and the complexity of the flowchart looping. The total length of the program



SUBROUTINES USED BY MORE THAN THREE OTHER SUBROUTINES - MATMUL
 RADEG
 DEGRAD
 RADM
 RADN

Figure 5-1
 System Flowchart

is approximately 1200 Fortran statements, with approximately 600 additional comment statements.

Main Program

The main program is used primarily to input the initial data and designate the various options that a particular run will have. The various parameters and branching instructions that are input are as follows:

- rate of rotation of earth,
- semi-major axis of reference ellipsoid,
- semi-minor axis of reference ellipsoid,
- translation components of reference ellipsoid,
- accelerometer sensitivities,
- minimum torques to gyro torquers,
- drift rates of gyros,
- accelerometer biases,
- cross product loop time interval,
- acceleration measurement interval,
- moving or stationary mode option,
- total time for stationary run,
- number of legs in traverse (maximum 5)
- ellipsoidal coordinates of points in traverse,
- maximum velocity attainable,
- time interval between ZUPT's
- time required to perform the update,
- Kalman filter or no Kalman filter,
- adjust coordinates using ZUPT procedure of Section 3.6
or do not adjust coordinates,

- alignment or no alignment of platform at a ZUPT,
- covariance matrix of initial latitude and longitude,
- variance of the observed ZUPT velocities,
- variance of initial orientation,
- variance of observed acceleration,
- variance of gyro drift rate,
- time between application of the prediction equations,
- option of zeroing or not zeroing the state vector at a ZUPT.

Subroutine LLISSS

This subroutine is the main subroutine and directs the execution of the simulation program. There are two main loops in this routine, namely, the cross product loop and the acceleration measuring loop. The cross product loop determines how often the mechanization equations (3-37) are applied. The acceleration measuring interval loop determines how often an acceleration is measured and converted to a change in velocity. The acceleration-time curve between measurements is assumed to be linear, whereas the actual curve is non-linear with the integration of the acceleration being of an analogue variety. Testing, using acceleration intervals of .008 seconds with cross product loops every .016 seconds compared to accelerations measured every .016 seconds showed that the coordinate difference after 90 minutes of operation was less than 0.1 centimetres in all three coordinates. Tests comparing the .008 second interval with lower time intervals (to .000 1 seconds) showed final coordinate differences over 90 minutes of even less than the above comparison.

The .008 second time interval for acceleration measurements and .016 second cross product loop time interval are used throughout this report.

Subroutine PLHXYZ

This subroutine computes the drift rotation matrix, R_{DR} , that is used to account for the gyro drifts. The drift rotation matrix is applied in the subroutine GYRO and is used at the end of every cross product loop time interval. The implicit assumption is that the rotation matrix formed here does not depend on the sequence in which the various drifts of the individual gyros are applied. For drifts of 10 seconds of arc per hour the rotation matrix so formed is accurate to 2×10^{-10} and does not produce any systematic error problems in the simulation model.

Subroutine ROTATE

This subroutine computes the coordinate system rotation matrices described in Appendix II.

Subroutine GRAV67

This subroutine computes the normal gravity at the desired point using equation (2-16). The normal gravity must be computed in the generation of the data and in the mechanization as well.

Subroutine XYZADJ

The purpose of this subroutine is to shift the input traverse points so that an integer number of cross product loops

may be instrumented in the moving platform simulations. It is this routine that defines when the accelerations take place, when there is constant velocity, and finally when ZUPT's take place. All computations are done in the Earth frame for this routine.

Function DIST

This function computes the distance between two points.

Subroutine MOVE

This subroutine generates the accelerations $[\ddot{X}, \ddot{Y}, \ddot{Z}]_{RE}^T$ of equation (3-14) and the true velocities $[\dot{X}, \dot{Y}, \dot{Z}]_{RE}^T$ in the Rotating Earth frame, as well as the true position $[X, Y, Z]_E^T$ of the platform in the Earth frame. This subroutine is called only if the platform is moving over the surface of the earth. The true position is output in both the ellipsoidal coordinates and Earth frame coordinates.

Subroutine XYZPLH

This subroutine converts the Earth frame cartesian coordinates to the latitude, longitude, and height of the chosen reference ellipsoid.

Subroutine GENDAT

If the platform is stationary this subroutine computes the normal gravity at the point. The normal gravity in the Z_{LL} or height channel is the only component sensed if the axes are ideally aligned and stationary.

When the platform is moving GENDAT uses the data supplied by subroutine MOVE to compute the true accelerations along the ideally

aligned Local Level axes. The theory behind the generation of accelerations for the moving platform must be expanded to fully appreciate the simulation program. Using equation (3-9) two expressions may be written. The first for the specific force along the Local Level axes is written

$$\ddot{\vec{r}}_{LL} = \ddot{\vec{r}}_{LL} + 2\dot{\vec{\omega}}_{LL} \times \dot{\vec{r}}_{LL} + \dot{\vec{\omega}}_{LL} \times \dot{\vec{r}}_{LL} + \dot{\vec{\omega}}_{LL} \times \dot{\vec{\omega}}_{LL} \times \vec{r}_{LL} \quad (5-1)$$

and the second for the specific force along the Rotating Earth axes is

$$\ddot{\vec{r}}_{RE} = \ddot{\vec{r}}_{RE} + 2\dot{\vec{\omega}}_{RE} \times \dot{\vec{r}}_{RE} + \dot{\vec{\omega}}_{RE} \times \dot{\vec{r}}_{RE} + \dot{\vec{\omega}}_{RE} \times \dot{\vec{\omega}}_{RE} \times \vec{r}_{RE} \quad (5-2)$$

The specific force in the Inertial frame is

$$\ddot{\vec{r}}_I = R_I^{LL} \ddot{\vec{r}}_{LL} \quad (5-3)$$

for the Local Level system, and

$$\ddot{\vec{r}}_I = R_I^{RE} \ddot{\vec{r}}_{RE} \quad (5-4)$$

for the Rotating Earth system, where

$$R_I^{LL} = R_3(-\omega_S \Delta t) R_3(90 - \lambda) R_1(90 - \phi) \quad (5-5)$$

from equation (2-14), and

$$R_I^{RE} = R_3(-\omega_S \Delta t) \quad (5-6)$$

from equation (2-4).

Putting (5-4) equivalent to (5-3) and multiplying both sides by R_{LL}^I yields

$$\begin{aligned} \ddot{\vec{r}}_{LL} + 2\vec{\omega}_{LL} \times \dot{\vec{r}}_{LL} + \dot{\vec{\omega}}_{LL} \times \vec{r}_{LL} + \vec{\omega}_{LL} \times \vec{\omega}_{LL} \times \vec{r}_{LL} \\ = R_{LL}^I R_I^{RE} (\ddot{\vec{r}}_{RE} + 2\vec{\omega}_{RE} \times \dot{\vec{r}}_{RE} + \dot{\vec{\omega}}_{RE} \times \vec{r}_{re} + \vec{\omega}_{RE} \times \vec{\omega}_{re} \times \vec{r}_{re}) \end{aligned} \quad (5-7)$$

where the term $\dot{\vec{\omega}}_{RE} \times \vec{r}_{RE}$ goes to zero as it is assumed that the rotation rate of the earth is constant. The subroutine GENDAT computes the expression on the right hand side of (5-7) for the sensed accelerations along the ideally aligned Local Level axes.

Subroutine ATTOLL

This subroutine forms the rotation matrix that rotates data from the Rotating Earth axes to the Local Level axes. Using equation (2-13) the matrix is given as

$$\begin{aligned} R_{LL}^{RE} &= R_{LL}^I R_I^{RE} \\ &= R_1(90 - \phi) R_3(90 + \lambda) \end{aligned} \quad (5-8)$$

Subroutine DATROT

The purpose of this routine is to rotate the data of subroutine GENDAT from the ideal Local Level axes to the actual Local Level axes. The approach taken is to compute the direction cosines matrix relating

the two sets of axes. The first step in computing the matrix is to solve for the unit vectors of the ideal Local Level axes at time $t = i + 1$ in terms of the Local Level axes at the time of the last alignment $t = i$ by writing

$$\begin{bmatrix} u_X \\ u_Y \\ u_Z \end{bmatrix}_{RUV} = R_1(90 - \phi_i)R_3(\lambda_i - \omega_S \Delta t - \lambda_{i+1})R_1(\phi_{i+1} - 90) \begin{bmatrix} u_X \\ u_Y \\ u_Z \end{bmatrix}_{UV}, \quad (5-10)$$

where UV denotes the unit vectors along the Local Level axes at time $t = i + 1$, RUV denotes the rotated unit vectors, and $\Delta t = t_{i+1} - t_i$.

These rotated unit vectors are compared with the rotated unit vectors of the actual system computed using the rotation matrix from subroutine GYRO. The dot product, from function DOTPRO, solves for the direction cosines matrix that relates the ideal and actual Local Level axes and the data (accelerations) is subsequently rotated from the ideal axes to the actual axes.

Function DOTPRO

This function forms the dot product of two input vectors.

Subroutine GYRO

The purpose of this routine is to form the rotation matrix, used in subroutine DATROT, that obtains the unit vectors of the actual Local Level axes in terms of the Local Level axes at the time of the last alignment. The GYRO subroutine is called for every cross product loop and the necessary rotation matrix is computed as

$$\text{ROT}_{i+1} = R_{DR} R_1(\dot{\phi}\Delta t) R_2(-(\omega_S + \dot{\lambda})\Delta t \cos \phi) R_3(-(\omega_S + \dot{\lambda})\Delta t \sin \phi) \text{ROT}_i$$

3x3 3x3 (5-11)

where ROT_i is the identity matrix after a realignment of the platform and Δt is the cross product loop time interval.

Subroutine PDKAL

The subroutine PDKAL executes the prediction equations (4-1) and (4-6) using the matrices described in Section 4.2.

Subroutine TRNSTN

This subroutine forms the transition matrix as described in Figure 4.1.

Subroutine MATTNP

This subroutine computes the transpose of an input matrix.

Subroutine ZUPT

The purpose of this routine is to either mechanize the ZUPT procedure as described in Section 3.5 or, if the Kalman filter is implemented, mechanize the filtering equations of Section 4.1. It is here that the option to realign the platform at a ZUPT is performed. This is done by making the matrix ROT described in subroutine GYRO equal to the identity matrix before the next cross product loop is executed.

Subroutine KALMAN

This subroutine implements equations (4-10), (4-15) and (4-18) and finishes the Kalman updating procedure based on the observed velocity errors during the zero velocity update.

Subroutine CHOLD

This is a subroutine developed to take the inverse of a symmetric matrix and is described in Wells [1971].

Subroutine MATMUL

This routine multiplies two matrices.

Subroutine RADEG

RADEG converts radians to degrees, minutes, and seconds of arc.

Subroutine DEGRAD

DEGRAD converts from degrees, minutes, and seconds of arc to radians.

Function RADN

This function computes the prime vertical radius of curvature, equation (2-6).

Function RADM

This function computes the meridian radius of curvature, equation (2-7).

5.2 Position Errors Caused by Accelerometer Biases and Gyro Drifts

With the aid of the simulation program the effects of the accelerometer biases and gyro drifts on position errors may be readily described. This information could be used to isolate a mechanical error by examining the data output of the actual system under good test conditions and then combining the error sources in the simulation program to duplicate this output. There is of course some ambiguity, as different error sources may combine to manifest themselves as similar position error time curves.

5.2.1 Accelerometer Biases in the Stationary Mode

The first quantities to be examined here are the effects of the accelerometer biases on the Local Level system operating in a stationary mode. The coordinates of the assumed position are

$$\phi = 45^{\circ} 00' 0."000 \quad ,$$

$$\lambda = 45^{\circ} 00' 0."000 \quad ,$$

and

$$h = 100.00 \text{ metres.}$$

The accelerometer biases used are all $1 \times 10^{-5} \text{ m sec}^{-2}$ or 1 mgal.

Under the above assumptions the latitude error, longitude error, and height error graphs of Figures 5-2, 5-3, and 5-4 respectively were constructed. The simulation was run under perfect conditions and is depicted by means of the solid line in the Figures mentioned above.

The error in position under perfect conditions results almost entirely from the fact that the torquing of the gyros is one step behind the actual measured acceleration because of the discrete time interval required to execute the mechanization equations. This error is usually not discussed in the navigation literature because it is not important for position accuracies of 1 kilometre per hour, but for surveying accuracies in the order of a few metres the torquing problem is a primary error source. The delay in the torquing command results in a systematic error which affects the longitude and height channels because the only torquing commands for the stationary platform are about the Y_{LL} axis at a rate $(\omega_S + \dot{\lambda}) \cos \phi$ and about the Z_{LL} axis at a rate $(\omega_S + \dot{\lambda}) \sin \phi$ (see equation (2-15)). The torque about the X_{LL} axis, $-\dot{\phi}$, which if in error would introduce gravitation components into the Y_{LL} channel and hence cause a latitude error, is seen to cause very small latitude errors in Figure 5-2. The torques about the Y_{LL} and Z_{LL} axes, when in error, introduce gravitational components into the X_{LL} channel and the Z_{LL} channel and cause the error curves depicted in Figure 5-3 and Figure 5-4 for the perfect operation case.

At this point some remarks concerning the sinusoidal shape of the error curves in the horizontal channels X_{LL} and Y_{LL} are in order. The shape results from the following sequence. To begin, one has an error in acceleration sensed along either the X_{LL} or Y_{LL} channels. This error in acceleration is integrated into an error in velocity and hence into an error in the torques applied to the gyros. Eventually the error introduced in the platform orientation causes gravitational accelerations to enter into the channel where the acceleration

measuring error was made in the first place. These accelerations are acting in the opposite sense to the original error that caused the velocity error. These accelerations eventually correct the velocity error, but unfortunately the corrections overshoot and the whole process is repeated in the opposite sense. This sequence just described takes approximately 84 minutes and is often referred to as the Schuler frequency. For a more detailed description the interested reader is referred to, for example, Farrell [1976, pg. 24] or Britting [1971].

In examining the graphs it is evident that the Schuler frequency in the horizontal channels has been somewhat modified. This results from the unbounded condition that exists in the height channel (Figure 5-4). There it may be easily seen that the height error, even when assuming mechanically perfect operation, is exponential in form with an error of approximately 300 metres introduced after 90 minutes of operation in the stationary mode. In aircraft systems this 'unbounded' height error is bounded by introducing altimetry data to supplement the measured inertial accelerations. For ships at sea the vertical accelerometer is often omitted or the data gathered from it is used only to monitor gravitational variations. On land the use of frequent zero velocity updating will bound the height error as is demonstrated in the next section.

Turning to the effects of the accelerometer biases in the stationary mode it can be seen that a Z_{LL} accelerometer bias significantly affects the latitude, longitude and height errors. The errors in vertical velocity become so large that the cross product terms $-\dot{h}\ddot{\phi}$, in the Y_{LL} channel, and $\dot{h}(\dot{\lambda} + 2\omega_S)\cos\phi$, in the X_{LL} channel, introduce large errors in the computation of the latitude and longitude.

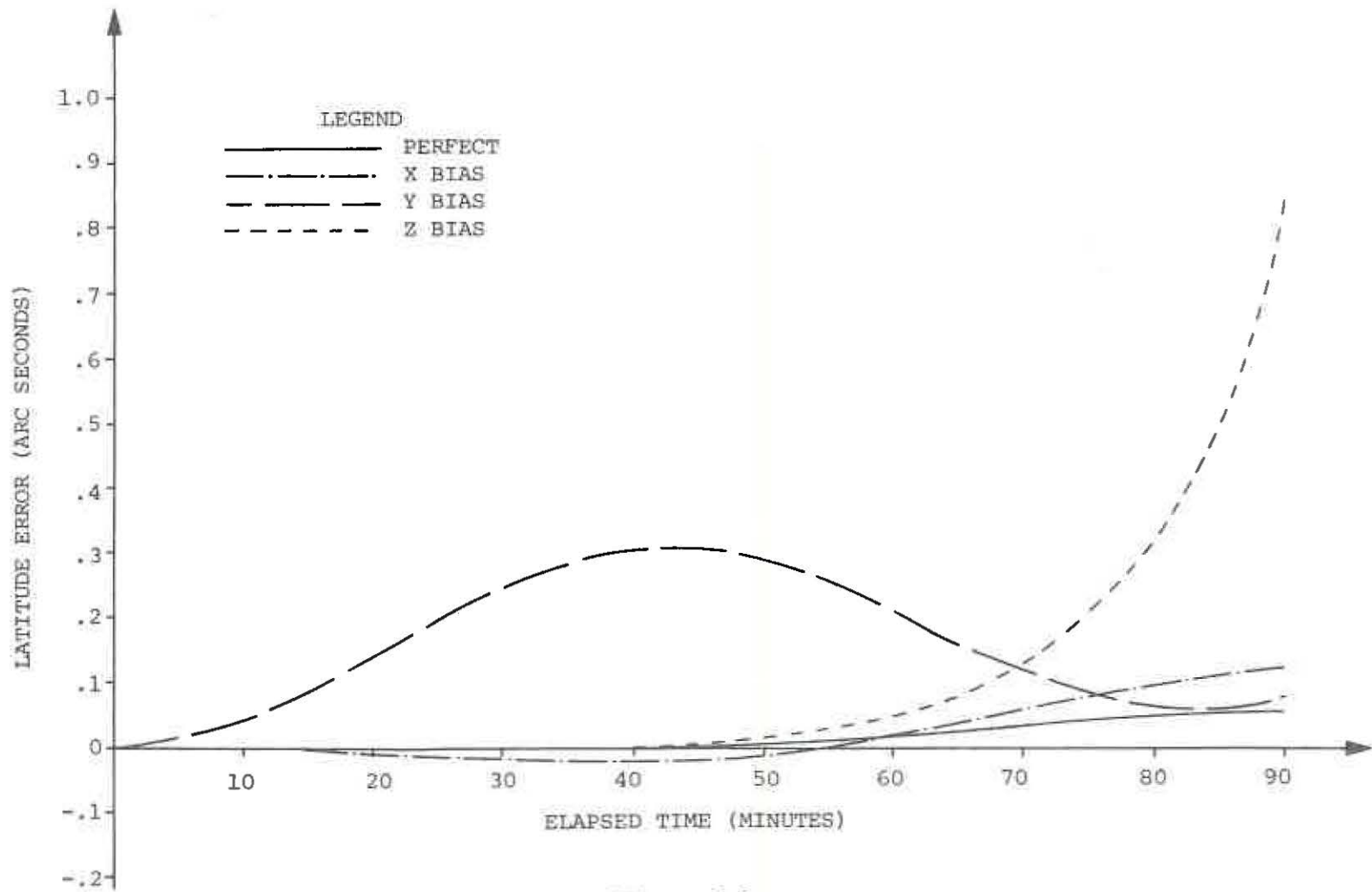


Figure 5-2
Accelerometer Biases - Latitude Error - Stationary Mode

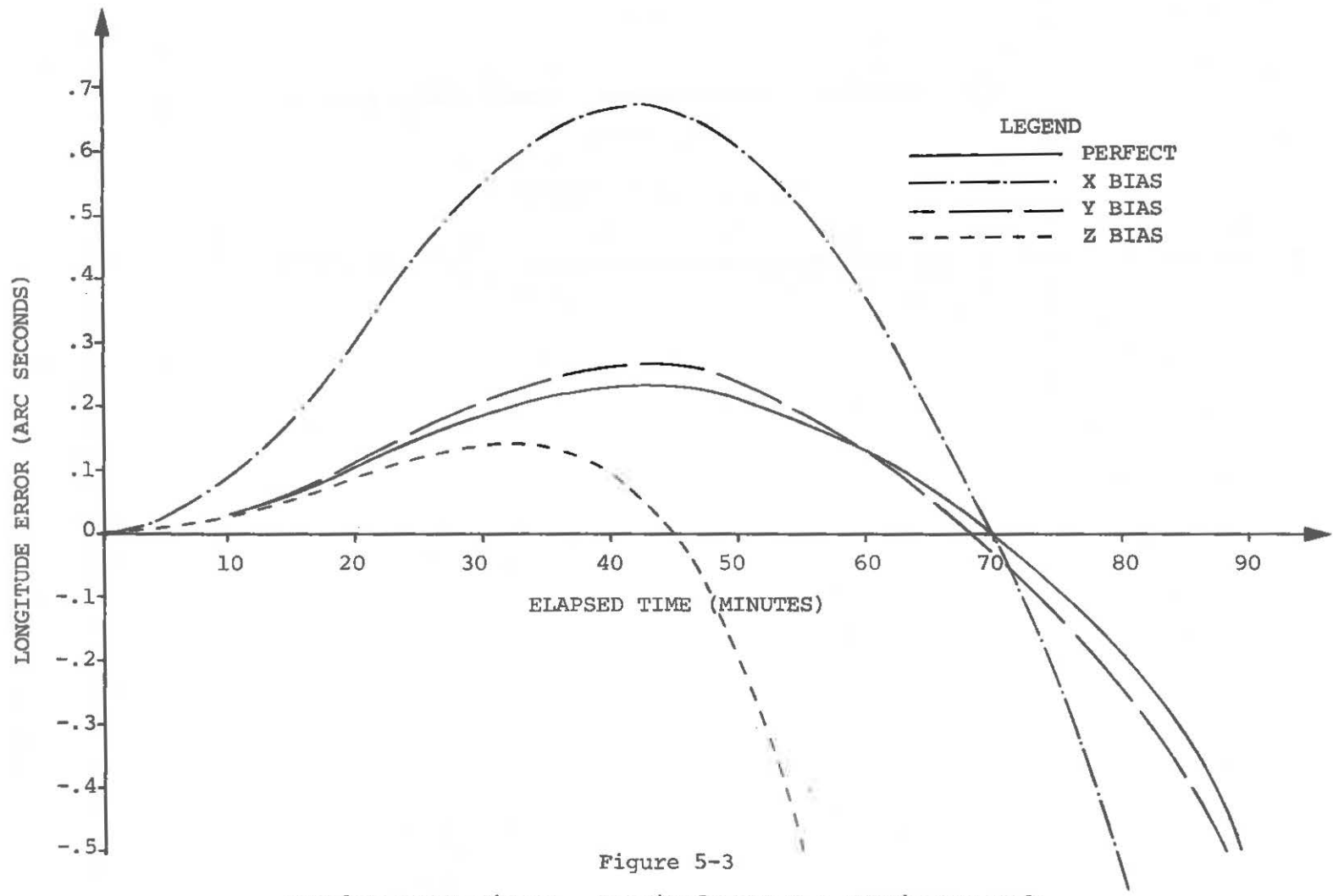


Figure 5-3
Accelerometer Biases - Longitude Error - Stationary Mode

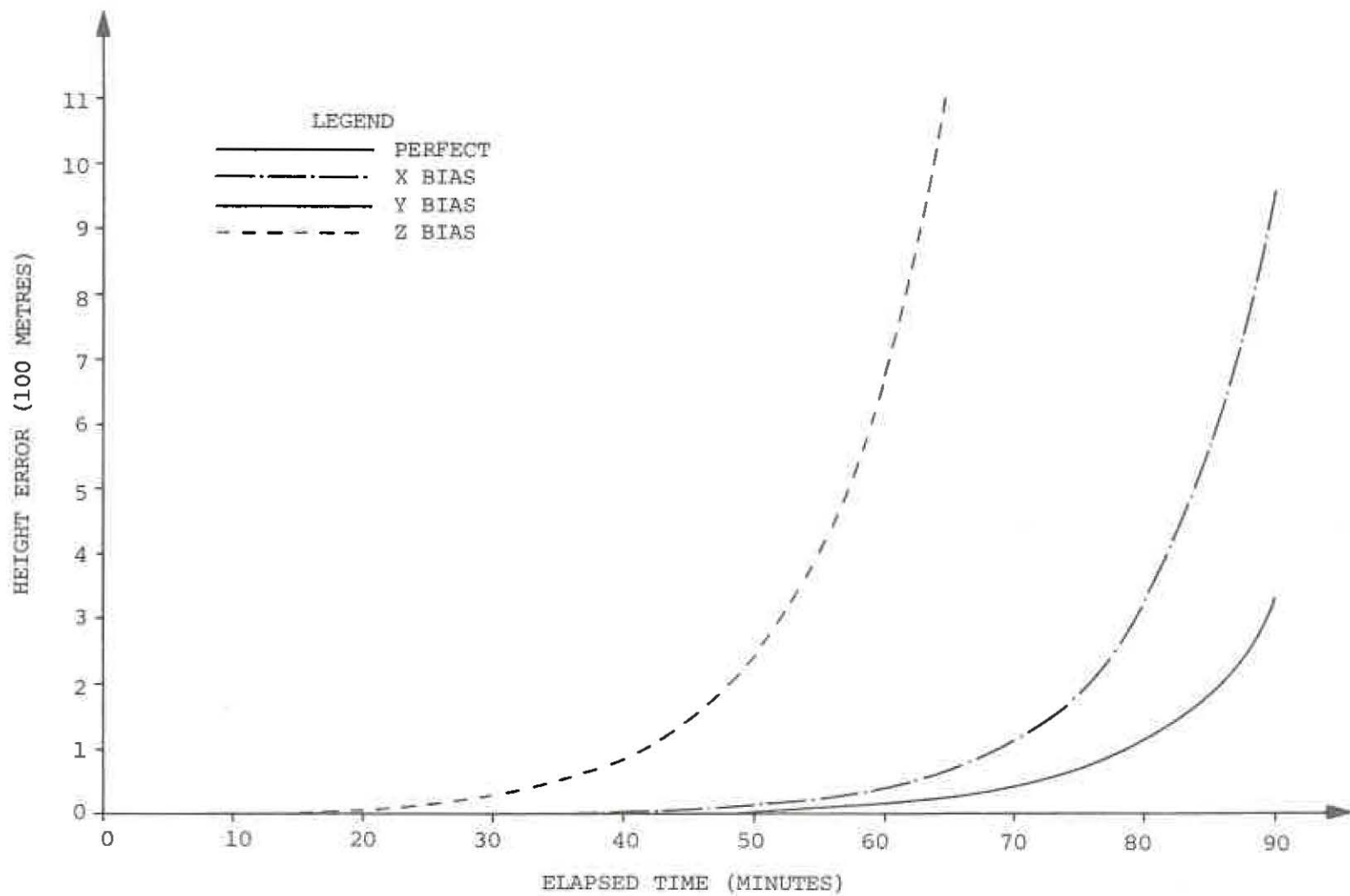


Figure 5-4
Accelerometer Biases - Height Error - Stationary Mode

In examining Figure 5-2 it can be seen that the y_{LL} accelerometer bias is the most critical up to the 70 minute mark, because this bias enters directly into the latitude computation. Similarly from Figure 5-3 it is evident that the x_{LL} accelerometer bias is the largest contributor to the longitude error up to about 50 minutes as this bias enters directly into the longitude computation.

5.2.2 Gyro Drifts in the Stationary Mode

The same type of analysis has been made on the contribution of the gyro drifts to the position error. The gyro drifts assumed for Figure 5-5, Figure 5-6 and Figure 5-7 are 1.5 arc seconds per hour. The stationary inertial system is again used with the same initial position as that used for the accelerometer biases.

In Figure 5-5 it can be seen that the gyro drift about the east or x_{LL} axis causes the largest latitude error. Britting [1971] has shown that all the latitude error curves resulting from gyro drift have a sine wave period of about 24 hours with the Schuler modulation, which has a period of about 84 minutes, superimposed on it. However, the simulation results will differ from the results obtained by Britting [1971] because of the more complete cross product interaction, the previously mentioned torquing lag, and of course, the inclusion of the vertical accelerometer with the resulting exponential height term error. These factors will greatly modify the position error curves for gyro drifts over periods longer than one hour. This may be seen in Figure 5-6 where the longitude error curves show the interaction of the height of z_{LL} channel (Figure 5-7) with the x_{LL} or longitude channel computations. Taking, for instance, the y drift position

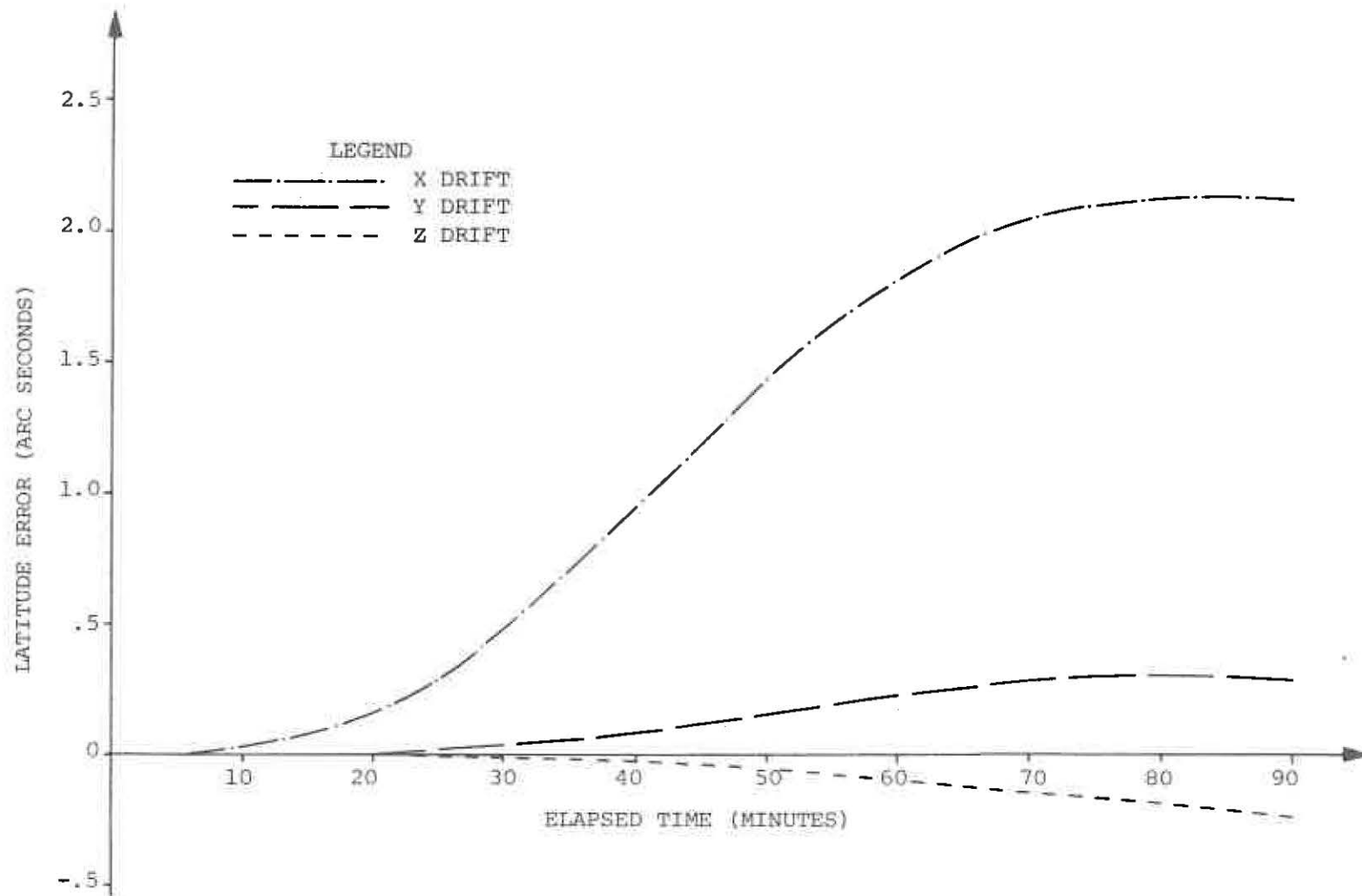


Figure 5-5
Gyro Drifts - Latitude Error - Stationary Mode

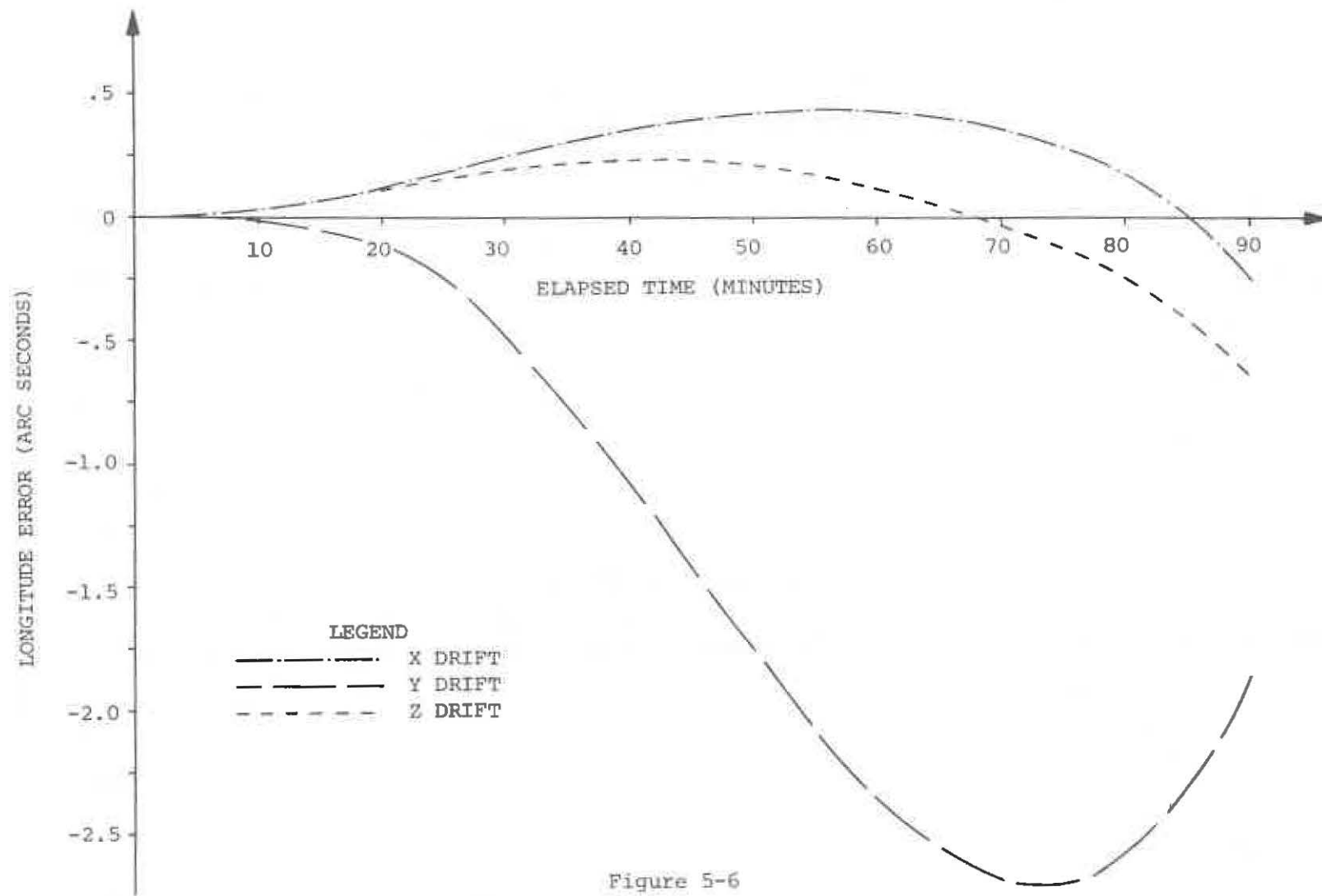


Figure 5-6
Gyro Drifts - Longitude Error - Stationary Mode

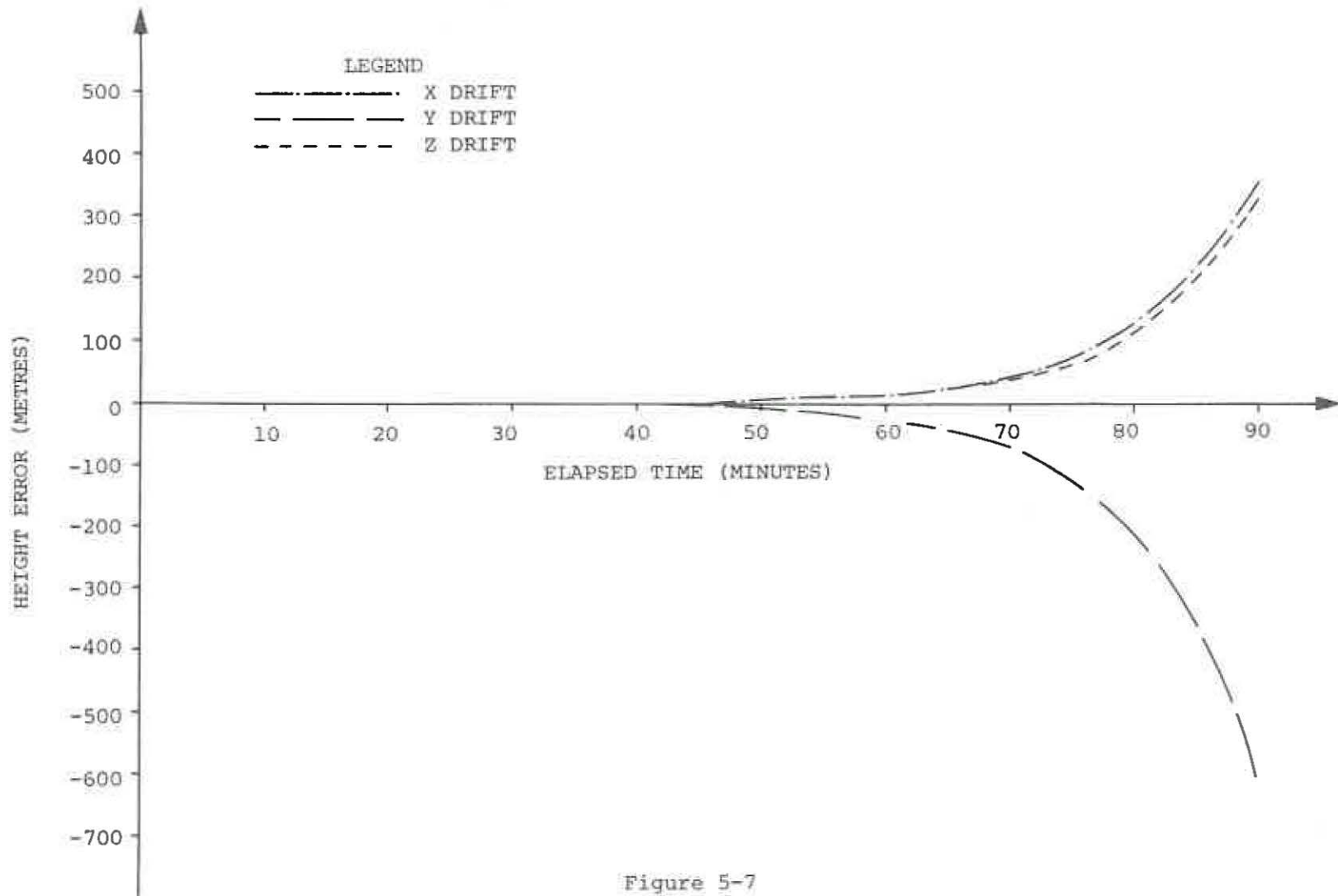


Figure 5-7
Gyro Drifts - Height Error - Stationary Mode

error curve in Figure 5-6 it can be seen that the exponential growth of the height error, and therefore height velocity, enters the longitude error curve because of the cross product term, $(\dot{\lambda} + 2\omega_S) \dot{z}_{LL} \cos \phi$, in equation (3-37). Without the inclusion of the height channel the longitude error would increase linearly in the negative direction [Britting, 1971].

5.2.3 Accelerometer Biases in the Moving Mode

Having examined the effects of the gyro drifts and accelerometer biases on the output of a stationary inertial system, the next step is to look at the more realistic case of the moving system. In this document only one test traverse is examined though any configuration of traverses may be handled by the simulation program. The following points are used for all discussions of the moving inertial system in this and the subsequent sections.

Point	Latitude			Longitude			Height Metres
	0	'	"	0	'	"	
1	45	0	0.000	45	0	0.000	100.00
2	45	3	59.993	45	3	59.993	100.00
3	45	7	59.992	45	7	59.992	100.00
4	45	11	59.998	45	11	59.998	100.00
5	45	15	59.994	45	15	59.994	100.00
6	45	19	59.998	45	19	59.998	100.00

Traverse Points

Table 5-1

It should be noted that the above points have been shifted from the input data to insure that an integer number of cross product loops could be mechanized, when moving between them. The maximum velocity

attainable by the vehicle was chosen to be 72 kilometres per hour and the time taken to go from 0 to 72 or from 72 to 0 kilometres per hour was taken to be 30 seconds. With the assumption of constant acceleration the acceleration of the vehicle was $\pm 0.666\ 67\ \text{m}\ \text{sec}^{-2}$. It should be noted that the simulation is programmed to have the vehicle come to a stop at each traverse point.

The average distance between the points in Table 5-1 is approximately 9 kilometres and the total traverse length is approximately 45 kilometres. Under the velocity and acceleration assumptions listed above, the vehicle takes about 40 minutes to complete the traverse.

Using the same accelerometer biases as for the stationary mode namely, $1 \times 10^{-5}\ \text{m}/\text{sec}^2$; the moving system was simulated and the results are depicted in Figures 5-8 to 5-10.

Examining the Figures it can be seen, that in this traverse the errors manifest themselves almost identically to the stationary mode results depicted in Figures 5-2 to 5-4.

5.2.4 Gyro Drifts in the Moving Mode.

Under the same traverse conditions as described in Section 5.2.3 the effects of the gyro drifts on position error were examined. The gyro drifts were assumed to be 1.5 arc seconds per hour and the results are depicted in Figures 5-11 to 5-13.

The chosen azimuth of the traverse of approximately 45 degrees and the low vehicle velocities are the reason that the drifts and biases show very little change in the moving mode.

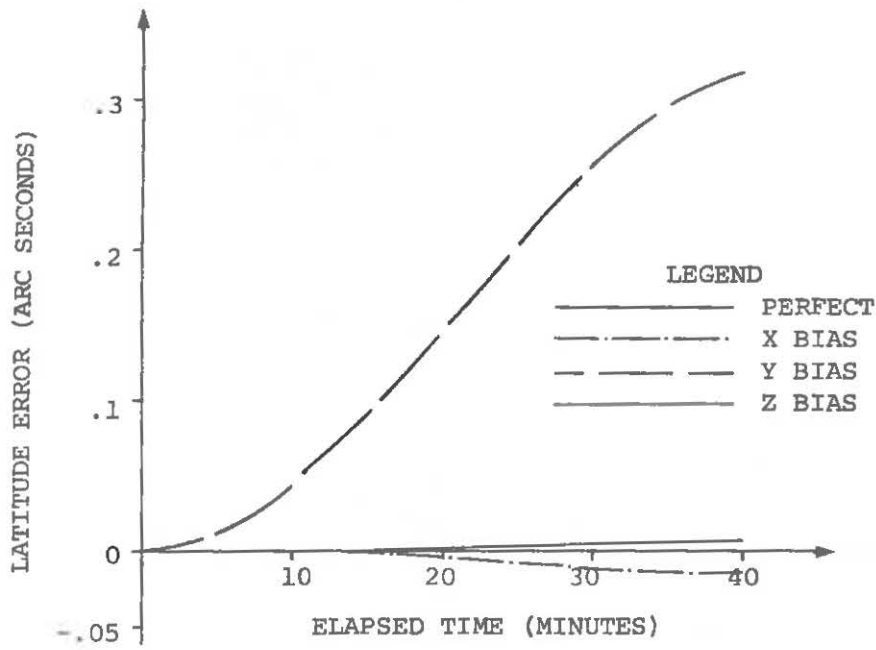


Figure 5-8

Accelerometer Biases - Latitude Error - Moving Mode

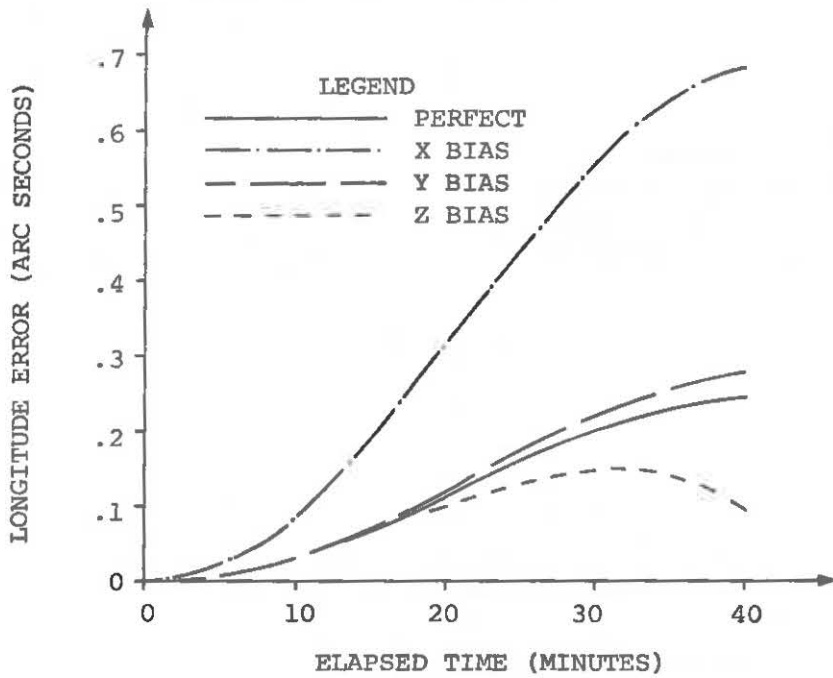


Figure 5-9

Accelerometer Biases - Longitude Error - Moving Mode

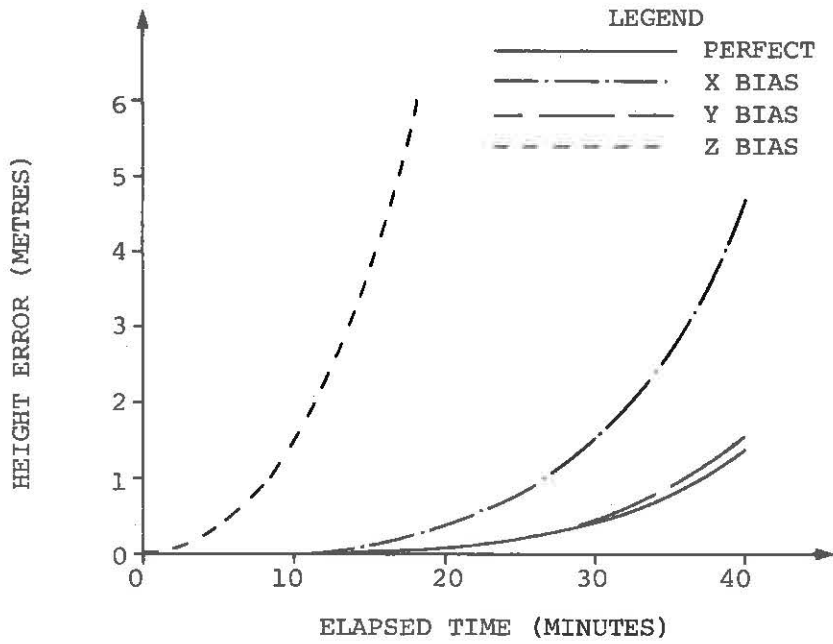


Figure 5-10
Accelerometer Biases - Height Error - Moving Mode

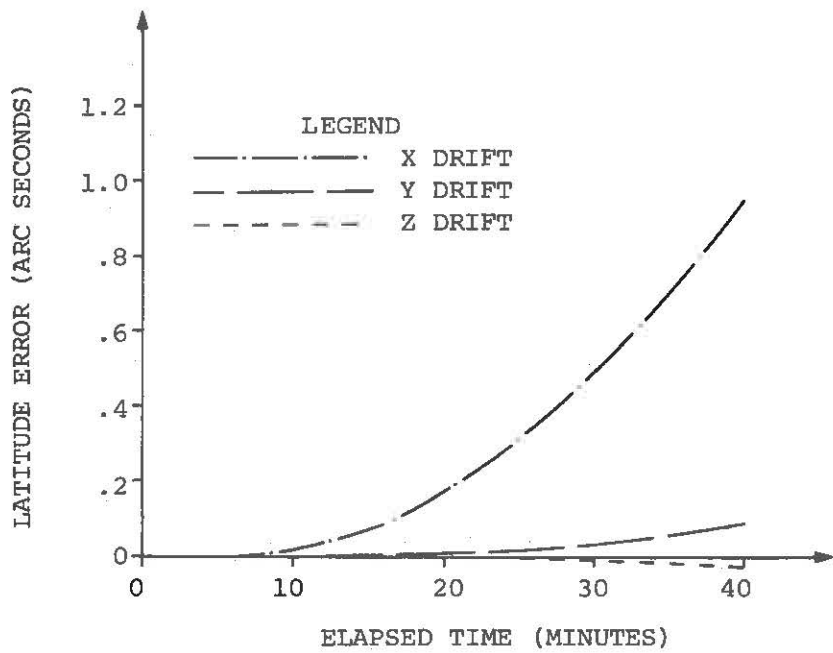
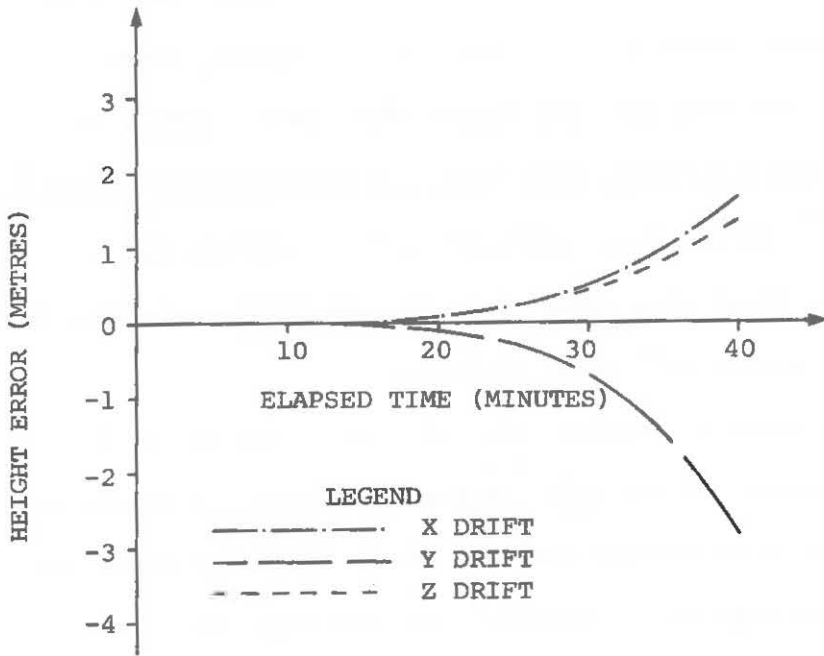
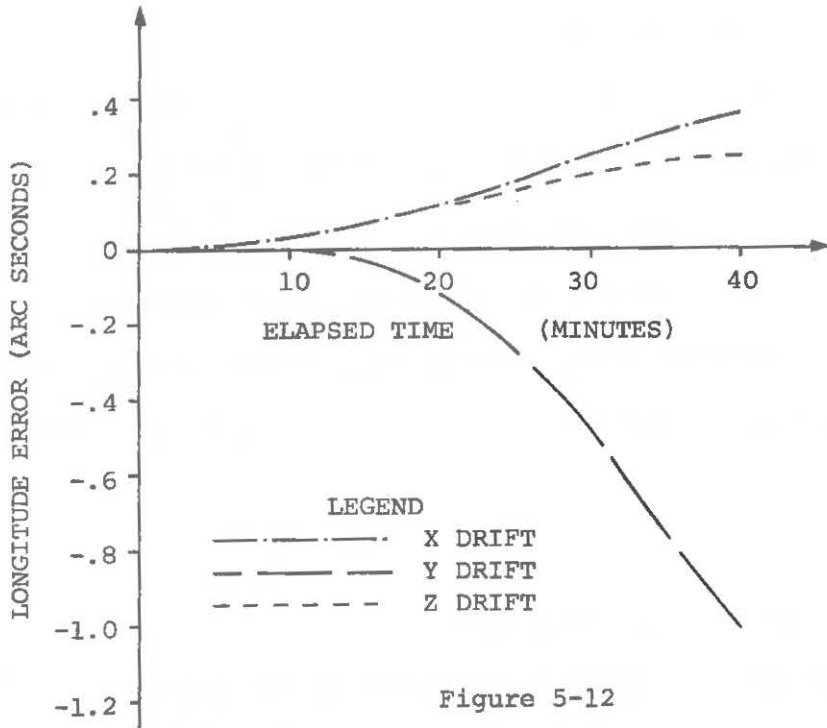


Figure 5-11
Gyro Drifts - Latitude Error - Moving Mode



5.3 Zero Velocity Update Simulation

To obtain better position error results, zero velocity updates are often used. The aim of this section is to show the results obtained using the simple ZUPT described in Section 3.6 and then show the results obtained using the Kalman ZUPT technique as described in Section 4.2. It is from the Kalman filter results that we obtain the first predicted accuracy results for the Local Level inertial survey system.

5.3.1 Simple ZUPT in the Stationary Mode.

Using the ZUPT procedure as described in Section 3.6, simulation runs were made to test the adequacy of the model. There are four simulation cases compared in Tables 5-2 to 5-5. CASE 1 is the simulation of the stationary platform with no system errors. Case 2 is the same run only with the simple ZUPT used. CASE 3 is the simulation of the stationary mode with all accelerometer biases of $1 \times 10^{-5} \text{ m sec}^{-2}$ and all gyro drifts of 1.5 arc seconds per hour included. The final case (CASE 4) is the simulation as described by CASE 3 with the simple ZUPT being utilized.

The time interval between each ZUPT was taken to be 300 seconds and the duration of the ZUPT, where the velocity average is obtained, was taken to be twenty seconds. These values are used for the ZUPTs in all the remaining sections. For the stationary cases the same initial point used in Section 5.2.1 is retained.

Commencing with the latitude error, Table 5-2, it may be seen that the simple ZUPT can be quite effective at eliminating the position error.

ELAPSED TIME (seconds)	LATITUDE ERROR (arc seconds)			
	CASE 1	CASE 2	CASE 3	CASE 4
320	.000 0	.000 0	.015 6	-.000 8
640	-.000 3	.000 0	.073 5	-.001 3
960	-.000 8	.000 0	.185 5	-.001 4
1280	-.001 6	.000 1	.355 8	-.001 3
1600	-.002 3	.000 1	.580 3	-.000 8
1920	-.002 5	.000 1	.846 6	-.000 1
2240	-.001 8	.000 1	1.136 5	.000 8
2560	.000 3	.000 2	1.427 9	.002 0
2880	.004 2	.000 2	1.698 7	.003 3
3200	.010 0	.000 2	1.930 0	.004 9

Table 5-2

Simple ZUPT - Latitude Error - Stationary Mode

It is easily seen that the gyro drifts and accelerometer biases tend to contaminate the velocity averaging during a ZUPT making the adjusted coordinates of CASE 4 much worse than the adjusted coordinates in CASE 2, where no systematic errors were introduced. Even with all the biases and drifts CASE 4 shows a maximum error of about 15 cm in horizontal position after 3200 seconds as opposed to 58 metres if the system went unchecked as in CASE 3. The longitude adjustment is not quite as good as the latitude adjustment with simple ZUPT's but again the results are favourable as can be seen in Table 5-3.

ELAPSED TIME (seconds)	LONGITUDE ERROR (arc seconds)			
	CASE 1	CASE 2	CASE 3	CASE 4
320	.009 3	.000 4	.021 8	.003 1
640	.035 9	.000 8	.064 9	.005 4
960	.075 4	.001 1	.094 6	.006 9
1 280	.121 9	.001 4	.078 3	.007 8
1 600	.167 9	.001 7	-.010 7	.008 2
1 920	.206 1	.002 0	-.191 2	.007 9
2 240	.230 5	.002 2	-.473 0	.007 2
2 560	.236 8	.002 5	-.861 1	.006 1
2 880	.223 4	.002 7	-1.361 2	.004 5
3 200	.190 8	.002 9	-1.992 7	.002 5

Table 5-3

Simple ZUPT - Longitude Error - Stationary Mode

With no systematic errors the maximum longitude error using simple ZUPT's is about 6 cm in horizontal position. With all biases and drifts, the maximum longitude error using simple ZUPT's is about 18 cm. Perhaps the most pleasing result of the simple ZUPT is that the height position error can be effectively bounded as indicated in Table 5-4.

ELAPSED TIME (seconds)	HEIGHT ERROR (metres)			
	CASE 1	CASE 2	CASE 3	CASE 4
320	.002	-.001	.400	.002
640	.019	-.002	1.744	.006
960	.066	-.003	4.469	.011
1 280	.168	-.003	9.433	.017
1 600	.358	-.004	18.200	.025
1 920	.697	-.005	33.544	.033
2 240	1.285	-.005	60.365	.043
2 560	2.302	-.006	107.280	.054
2 880	4.063	-.006	189.420	.065
3 200	7.126	-.007	333.335	.078

Table 5-4

Simple ZUPT - Height Error - Stationary Mode

The maximum position error after adjustment is seen to be less than 8 cm for the case when all biases and drifts were present.

From the tabulated results in the stationary mode it appears that the simple ZUPT procedure is capable of keeping the position error in the decimetre range. The major shortcoming of the simple ZUPT model is the total lack of any statistical estimate of the position error which is one of the major reasons that the more sophisticated Kalman model must be used. This is somewhat analagous to the compass rule adjustment of a conventional traverse as opposed to a least squares adjustment. The compass rule adjustment yields good final coordinates but unfortunately no statistical estimate of the quality of the computed positions.

5.3.2 Simple ZUPT in the Moving Mode.

Again using the simple ZUPT procedure of Section 3.6 simulation runs of the moving system were made. The coordinates of the traverse points are the same as those given in Section 5.2.3. As mentioned in the preceeding section the ZUPT duration is 20 seconds and the time interval between ZUPT's is 300 seconds. There is also a ZUPT executed at each traverse point, excluding the first one, and it is at each traverse point that the position error is computed and compared. The same maximum velocity and accelerations as described in Section 5.2.3 are used in the simulation runs of this section. Finally, four cases will be considered for the moving system. The first case has the system traversing with no biases and drifts. The second case is the same run as CASE 1 with the simple ZUPT of Section 3.6 applied. The third case involves all the accelerometer biases of $1 \times 10^{-5} \text{ m sec}^{-2}$

and all the gyro drifts of 1.5 arc seconds per hour. The final case is the repetition of CASE 3 with the addition of the simple ZUPT procedure. To make the comparison of the results from the moving and stationary systems possible, the following table of elapsed times to the various traverse points is provided. Also listed in the same table is the total distance traversed.

TRAVERSE POINT	ELAPSED TIME (seconds)	DISTANCE TRAVERSED (metres)
1	0	0
2	554.112	9 082.2
3	1 108.064	18 161.3
4	1 661.856	27 237.1
5	2 215.456	36 309.1
6	2 768.896	45 377.9

Table 5-5

Elapsed Time - Distance Traversed - Moving Mode

The first position error examined is the latitude error,

Table 5-6

TRAVERSE POINT	LATITUDE ERROR (arc seconds)			
	CASE 1	CASE 2	CASE 3	CASE 4
2	.001 0	-.000 4	.054 1	-.000 5
3	.002 2	.000 8	.260 2	-.000 1
4	.003 1	.001 2	.633 6	.000 8
5	.004 7	.001 6	1.118 2	.002 4
6	.009 2	.002 0	1.608 3	.004 5

Table 5-6

Simple ZUPT - Latitude Error - Moving Mode

The errors after the simple ZUPT application in CASE 2 are seen to be larger than for the equivalent case in the stationary mode, Table 5-2. This results from the fact that the moving mode introduces cross product terms of a higher magnitude, thereby reducing the linearity of the velocity-time error curve which is the underlying assumption for the validity of the simple ZUPT. The same reasoning accounts for the higher terms in CASE 4 when compared to the latitude error, under the same conditions, in the stationary mode, Table 5-2.

The corresponding longitude errors are given in Table 5-7.

TRAVERSE POINT	LONGITUDE ERROR (arc seconds)			
	CASE 1	CASE 2	CASE 3	CASE 4
2	.027 5	-.000 1	.053 5	.003 5
3	.098 7	-.000 2	.097 1	.005 4
4	.181 3	-.000 3	-.032 4	.006 0
5	.237 2	-.000 5	-.440 4	.005 3
6	.239 6	-.000 8	-1.170 5	.003 7

Table 5-7

Simple ZUPT - Longitude Error - Moving Mode

For the longitude error it can be seen that the moving mode yields smaller longitude errors in CASE 2 and CASE 4 than does the similar cases in TABLE 5-3 for the stationary mode. This is a result of the cross product terms, mentioned in the latitude error description above, having somewhat of a cancelling effect for this particular traverse.

Finally the height error results are tabulated for the four cases in Table 5-8.

TRAVERSE POINT	HEIGHT ERROR (metres)			
	CASE 1	CASE 2	CASE 3	CASE 4
2	-.001	-.012	1.240	-.003
3	.070	-.025	6.392	-.004
4	.322	-.036	20.509	-.003
5	1.003	-.048	57.697	-.002
6	2.751	-.060	155.498	.004

Table 5-8

Simple ZUPT - Height Error - Moving Mode

In Table 5-8 the simple ZUPT under the traverse conditions listed is able to correct the height error in CASE 4 with all the gyro drifts and accelerometer biases better than in CASE 2.

No general conclusions may be made as to the accuracy of the simple ZUPT unless all possible traverses with all combinations of biases and drifts were examined. This leads one to the use of Kalman filtering techniques which give not only the updated coordinates but also an estimate of their accuracy. This eliminates the need for a complete simulation of each traverse which would be extremely difficult for a real time system.

5.3.3 Kalman ZUPT in the Stationary Mode

The objective of this section is to demonstrate the capabilities of the Kalman filtering techniques by simulating the cases mentioned in Sections 5.3.1 and 5.3.2 with the filtering implemented. At the time of writing of this report detailed information on the accuracies of various components of the inertial surveying system were not forthcoming from the manufacturer. This has led to a number of assumptions being made so that the Kalman filter could be fully implemented.

The Kalman filter used in the simulation has been fully described in Section 4. It is seen there that the accelerations in the Z_{LL} or height channel have been omitted from the development. The reason for the omission is that the increased number of terms would make the solution for the transition matrix more difficult and therefore the detection of errors would be a more complex procedure. By setting up the Kalman filter of Section 4.2 the foundation for going to the additional Z_{LL} channel terms has been set. One option from here is to go to a two step procedure with two transition matrices and the correlation between the height channel and the horizontal channels neglected. The second and more difficult option is to derive the full transition matrix, with the height position error and height velocity error added to the state vector, equation (4-19).

To make the simulation of the Kalman ZUPT comparable to that of the simple ZUPT of the preceding Sections 5.3.1 and 5.3.2, the height channel has been subjected to the simple ZUPT technique. This prevents the exponential growth of errors in that channel from contaminating the horizontal channel output.

For the stationary mode the same initial coordinates as in Section 5.2.1 are used. The initial covariance matrix on position is

$$C_{\phi, \lambda} = \begin{bmatrix} 1 \times 10^{-3} \text{ arc sec}^2 & 0 \\ 0 & 1 \times 10^{-3} \text{ arc sec}^2 \end{bmatrix}$$

The variance on initial misorientation is taken to be 100 arc sec^2 and the initial variance on velocity is taken to be $4.197 \times 10^{-10} \text{ arc sec}^2 \text{ sec}^{-2}$ for the latitude velocity and 8.338×10^{-10}

arc sec² sec⁻² for the longitude velocity. These velocity variances are derived from the horizontal channel velocity variance of $4 \times 10^{-7} \text{ m}^2 \text{ sec}^{-2}$.

Using the above values the matrix C_{X^0} (equation 4-8) would be given by

$$C_{X^0} = \begin{bmatrix} 100.0 \text{ arc sec}^2 & & & & & & & \\ & 100.0 \text{ arc sec}^2 & & & & & & \\ & & 100.0 \text{ arc sec}^2 & & & & & \\ & & & 0.001 \text{ arc sec}^2 & & & & \\ & & & & 0.001 \text{ arc sec}^2 & & & \\ & & & & & 4.197 \times 10^{-10} \text{ arc sec}^2 \text{ sec}^{-2} & & \\ & & & & & & 8.338 \times 10^{-10} \text{ arc sec}^2 \text{ sec}^{-2} & \end{bmatrix}$$

Using a variance on the observed acceleration (every .016 seconds) of $1.0 \times 10^{-8} \text{ m}^2 \text{ sec}^{-4}$, and a variance on the drift random noise of $2.5 \times 10^{-6} \text{ arc sec}^2$ (every .016 seconds), the model error matrix (4-69) is given using equations (4-64) through (4-68) as

$$P_m^{-1} = \begin{bmatrix} 1.575 \times 10^{-4} \text{ arc sec}^2 & & & & & & & \\ & 1.575 \times 10^{-4} \text{ arc sec}^2 & & & & & & \\ & & 1.575 \times 10^{-4} \text{ arc sec}^2 & & & & & \\ & & & 0 & & & & \\ & & & & 0 & & & \\ & & & & & 1.692 \times 10^{-12} \text{ arc sec}^2 \text{ sec}^{-2} & & \\ & & & & & & 3.362 \times 10^{-12} \text{ arc sec}^2 \text{ sec}^{-2} & \end{bmatrix}$$

where the time between Kalman predictions is 1.008 seconds (63 cross product loops of .016 seconds).

Using the values described above the stationary case was simulated under the same conditions as those used in the simple ZUPT of Section 5.3.1. That is, the time interval between each ZUPT is 300 seconds and the duration of a ZUPT is 20 seconds. CASE 5 assumes no gyro drifts and accelerometer biases and is directly comparable to CASE 1 and CASE 2 of Section 5.3.1. CASE 6 assumes gyro drifts of 1.5 arc seconds in all channels and accelerometer biases of 1×10^{-5} m sec⁻² in all channels. Because of the assumed drifts, the drift variance added at each zero velocity update is given by (equation 4-75)

$$\sigma_D^2 = (2 \text{ arc sec} \cdot t)^2$$

where t is the time since the last alignment. The latitude and longitude position errors are given in Table 5-9 and these values are directly comparable to the results for the simple ZUPT which are tabulated in Table 5-2 and Table 5-3.

ELAPSED TIME (seconds)	LATITUDE ERROR (arc seconds)		LONGITUDE ERROR (arc seconds)	
	CASE 5	CASE 6	CASE 5	CASE 6
320	.000 0	-.001 1	.000 3	.001 9
640	.000 0	-.000 3	.000 8	.004 6
960	.000 0	.001 7	.001 2	.005 3
1 280	-.000 1	.002 8	.001 3	.005 5
1 600	-.000 1	.003 6	.001 3	.005 4
1 920	-.000 1	.003 9	.001 0	.005 0
2 240	-.000 1	.003 6	.000 5	.004 9
2 560	-.000 1	.002 6	-.000 1	.005 3
2 880	-.000 1	.001 0	-.000 7	.006 6
3 200	-.000 1	-.001 2	-.001 2	.008 9

Table 5-9

In comparing the three tables it is seen that the simple ZUPT and Kalman ZUPT techniques demonstrate position errors of the same magnitude. However the Kalman technique does give the essential covariance matrix of the state vector. At the 3 200 second point the covariance matrix of the state vector is

$$C_X^{\wedge} = \left[\begin{array}{cccccccc} 2.385 & & & & & & & \\ -2.59 \times 10^{-4} & 2.388 & & & & & & \\ -6.55 \times 10^{-6} & .407 & 68.484 & & & & & \\ -6.57 \times 10^{-4} & -8.37 \times 10^{-6} & -8.29 \times 10^{-5} & 1.484 \times 10^{-3} & & & & \\ 4.60 \times 10^{-9} & 2.03 \times 10^{-6} & -3.56 \times 10^{-7} & -2.59 \times 10^{-8} & 1.743 \times 10^{-3} & & & \\ -7.37 \times 10^{-6} & 1.14 \times 10^{-8} & 5.43 \times 10^{-8} & 4.84 \times 10^{-10} & -1.44 \times 10^{-8} & 4.190 \times 10^{-10} & & \\ -1.59 \times 10^{-6} & -1.03 \times 10^{-8} & -6.49 \times 10^{-8} & 1.53 \times 10^{-10} & 0.76 \times 10^{-8} & 3.946 \times 10^{-16} & 8.32 \times 10^{-10} & \end{array} \right]$$

SYMMETRIC MATRIX

where the units are the same as those of C_{X^0} (equation (5-12)).

The important point to note is that the variance on the latitude and longitude has gone from 1×10^{-3} arc sec² to 1.731×10^{-3} arc sec and 2.031×10^{-3} arc sec² respectively after 3 200 seconds operation.

This represents a relative latitude and longitude variance of approximately 2.5 m^2 under the conditions listed above ($.7 \text{ m}^2$ if original point is perfectly known). In the C_X^{\wedge} matrix it is observed that the azimuth misorientation variance is much larger than the other two misorientation variances. This results from the fact that the horizontal velocities observed during velocity updates are more weakly related to the azimuth misorientation than the $\psi_{Y_{LL}}$ and $\psi_{X_{LL}}$ misorientation.

Table 5-10 provides an outline of how the position standard deviations have increased with time.

ELAPSED TIME (seconds)	Standard Deviation (arc sec)	
	LATITUDE	LONGITUDE
0	.031 6	.031 6
320	.032 2	.032 6
640	.033 1	.034 2
960	.033 9	.035 7
1 280	.034 9	.037 1
1 600	.035 9	.038 6
1 920	.037 0	.039 9
2 240	.038 1	.041 3
2 560	.039 2	.042 6
2 880	.040 4	.043 8
3 200	.041 6	.045 1

Table 5-10

Latitude and Longitude Standard Deviation - Stationary Mode

It may be seen that the increase in standard deviation is quite linear with time for both latitude and longitude. The reason for the standard deviations being significantly larger than the position error when comparing Table 5-10 to Table 5-9 is that the random noise is not added to the accelerometer observations and gyro pickoff observations in the present simulation which makes the position error appear somewhat better than it should. This is also the case for the moving mode in the next section.

5.3.4 Kalman ZUPT in the Moving Mode

The Kalman filter was also simulated in the moving mode for the open traverse as shown in Table 5-1. The variances on the various input parameters were identical to those used in the stationary mode, Section 5.3.3, and the Kalman prediction interval of 1.008 seconds was also used. The latitude and longitude position errors are given in Table 5-11 and these values are directly comparable to the results

from the simple ZUPT which are tabulated in Table 5-6 and Table 5-7.

The two cases examined are identical to those described in Section 5.3.3.

TRAVERSE POINT	LATITUDE ERROR (arc Seconds)		LONGITUDE ERROR (arc seconds)	
	CASE 5	CASE 6	CASE 5	CASE 6
2	.000 4	.000 5	.000 0	.003 2
3	.000 7	.003 0	.000 0	.004 0
4	.000 9	.004 6	-.000 7	.004 0
5	.001 1	.004 5	-.001 8	.004 3
6	.001 3	.002 5	-.003 3	.006 6

Table 5-11

Kalman ZUPT -Latitude and Longitude Error - Moving Mode

Again in comparing the three tables it is seen that the simple ZUPT and Kalman ZUPT techniques demonstrate position errors of the same magnitude. The covariance matrix of the state vector at point 6 is

$$C_X = \begin{bmatrix} 3.181 & & & & & & & & & \\ -4.96 \times 10^{-6} & 3.186 & & & & & & & & \\ -1.08 \times 10^{-3} & .549 & 69.435 & & & & & & & \\ -9.44 \times 10^{-6} & -1.44 \times 10^{-3} & - .114 & 1.731 \times 10^{-3} & & & & & & \\ 6.92 \times 10^{-4} & 2.18 \times 10^{-7} & -1.22 \times 10^{-4} & -3.82 \times 10^{-5} & 2.031 \times 10^{-2} & & & & & \\ -7.29 \times 10^{-9} & 8.12 \times 10^{-8} & 3.49 \times 10^{-7} & 6.72 \times 10^{-8} & -2.68 \times 10^{-10} & 4.194 \times 10^{-10} & & & & \\ -1.14 \times 10^{-6} & -1.02 \times 10^{-8} & -9.19 \times 10^{-7} & 2.73 \times 10^{-10} & 1.34 \times 10^{-7} & 1.88 \times 10^{-17} & 8.33 \times 10^{-10} & & & \end{bmatrix}$$

SYMMETRIC MATRIX

where the units are the same as those of C_{X_0} (equation (5-12)).

From the above covariance matrix one can see that the variance on the latitude and longitude has increased from 1×10^{-3} arc sec² to 1.484×10^{-3} arc sec² and 1.743×10^{-3} arc sec² respectively. This converts to an approximately 20 centimetre increase in the standard deviation over a 45 kilometre traverse of about 50 minutes duration. This represents a relative latitude and longitude variance of approximately 2.2 m^2 ($.44 \text{ m}^2$ if original point is perfectly known). The

standard deviation increase over the traverse period is shown in Table 5-12.

TRAVERSE POINT	ELAPSED TIME (seconds)	Standard Deviation (arc sec)	
		LATITUDE	LONGITUDE
1	0	.031 6	.031 6
2	554.112	.032 7	.033 5
3	1 108.064	.034 0	.035 7
4	1 661.856	.035 4	.037 8
5	2 215.456	.036 9	.039 8
6	2 768.896	.038 5	.041 8

Table 5-12

Latitude and Longitude Standard Deviation - Moving Mode

The results in Table 5-12 are similar to those of the stationary mode, Table 5-10, in that the increase over the traverse period is nearly linear. The reason for the slightly lower values of standard deviation in the moving mode (when using elapsed time comparison) is because there is a ZUPT at the end of each traverse leg in addition to the ZUPT every 300 seconds which strengthens the model because of the additional observations.

5.3.5 Time Interval Between ZUPT's

To obtain an estimate of how the time interval between ZUPT's affects the standard deviation of position, simulations of Local Level system were run with various time intervals in the stationary mode. The longitude standard deviation as it increases in time is depicted in Figure 5-14. The Figure indicates that the improvement in the standard deviation becomes less for the same decrease in the ZUPT interval as the time interval between ZUPTs

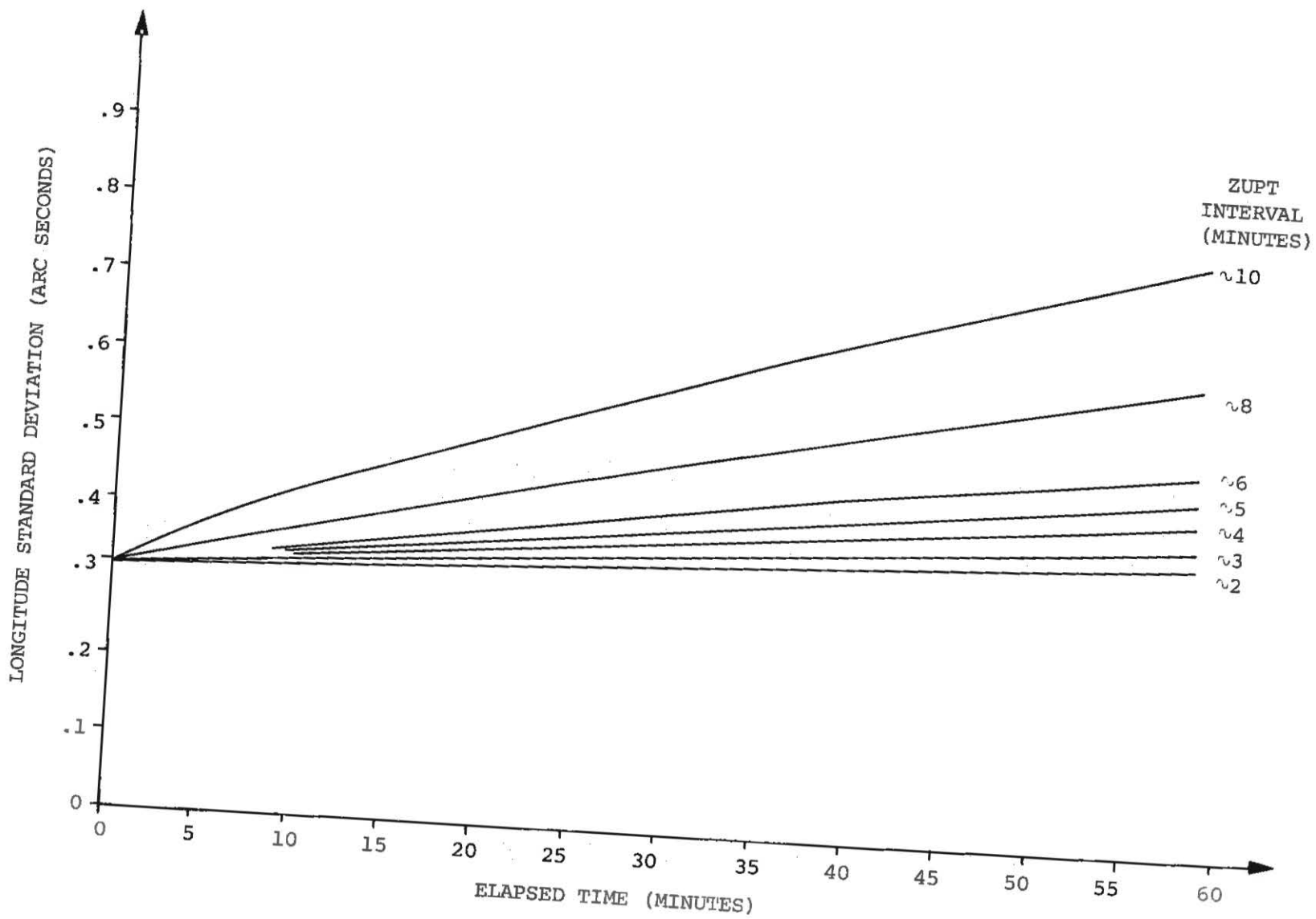


Figure 5-14
 Longitude Standard Deviation vs Time for Different Zupt Intervals

decreases. It would be up to the individual user to choose a ZUPT interval which meets the specifications of the survey, while still enabling fast efficient operation. The simulation program may be used along with the inertial manufacturer's specifications and the desired Kalman filter to select the proper update interval.

6. CONCLUSIONS AND RECOMMENDATIONS

This report is an investigation of the fundamental properties of the Local Level inertial survey system. The basic coordinate systems, operating principles, and necessary mechanization equations have been described and are incorporated in the simulation program. Some preliminary results have been stated in Section 5 and they indicate that some form of zero velocity updating is required to bound the system position and velocity errors during a survey mission. Empirical results indicate that the simple ZUPT procedure explained in Section 3.6 is as effective at bounding the errors as the more rigorous Kalman model developed in Section 4.2. Unfortunately the simple ZUPT procedure provides no indication of the accuracy of the output. The Kalman model does provide this information and it is here that the future of inertial system improvement rests. The Kalman filter used in this paper contains seven elements in the state vector, namely three misorientation unknowns, two position unknowns, and two velocity unknowns. The position and velocity unknowns incorporate only the horizontal channels (X_{LL}, Y_{LL}) of the Local Level system and neglect the vertical channel (Z_{LL}) . For three dimensional survey systems the vertical or height channel must be included in the state vector; making it a nine element state vector. The inclusion of the additional

two elements makes the solution for the transition matrix much more difficult and perhaps unstable [Britting, 1971, pg. 182] . The problem could perhaps be alleviated by forming two state vectors. The first would be as described in Section 4.2 and the second state vector would contain the three misorientation unknowns along with height and height velocity terms (5 element state vector). The disadvantage of such a system would be the loss of covariance information between the state vectors, and the loss of cross product interaction between the channels.

Because this report is an investigation of the fundamentals only, there are numerous recommendations for further investigation, namely:

- (i) To make more realistic evaluations of the system performance more information must be obtained with regard to the alignment and calibration procedures used by the manufacturers. In addition the accuracies of the various components must be clearly determined. Without this information no quantitative estimate of the obtainable accuracies is possible.
- (ii) The neglected terms in the linear differential equations leading to the Kalman filter transition matrix should be included and the errors resulting from the omission of the various terms should be quantified.
- (iii) The anomalous gravity field which has been neglected in this report must be modelled and inserted into the simulation to obtain estimates of the error introduced by its omission. After determining the contribution from this source, effort must be made to determine the best method of incorporating

the anomalous model into the actual system for real time computations. This will involve the modification of the Kalman procedure to include the anomalous terms as a priori information (additional information) in the case where the gravity field is assumed known. If the anomalous field is unknown there are problems involved in separating out the anomalous gravity field errors from the other systematic error sources.

- (iv) Simulation runs should be made to test for the best Kalman prediction interval, cross product loop interval, and gyro torquing interval for inertial survey systems. Along with this testing, the Kalman ZUPT interval should be examined as is done in Section 5.3.5.
- (v) The 9 element state vector as described previously should be modelled and tested in the simulation program. The two state vector procedure would most likely be the first step towards the inclusion of the height channel terms. There has already been research in the area of the extended filter with some researchers going as high as a 27 element state vector [Adams, 1977] for the Space Stabilized system.
- (vi) After the filter is properly instrumented and the anomalous gravity field included in the program, the simulation program should then be used as a preanalysis tool where the expected traverse configuration and anomalous gravity field characteristics similar to those in the traverse area are fed as input to the program. In this way time and money may be saved in the field work by knowing such things as the proper zero velocity update interval and the number of times the traverse must be run.

- (vii) Post mission smoothing must also be examined. The greatest problem here is the tremendous amount of data that would have to be stored to properly smooth the data. Further investigation might prove this unnecessary but extensive testing and analysis would be required. The minimum amount of data that must be stored is the position and its covariance matrix for each determined point. In this way a proper weighted average could be determined for the position by simply combining all solutions for the coordinates of the desired point. A more difficult problem to solve is the determination of the covariance terms linking two established points. These problems must be further analysed before the inertial surveyor may be used as a proper tool for network densification.
- (viii) The integration of inertial with other positioning devices such as Doppler satellite, land based hyperbolic and ranging systems [Gentry et. al., 1975] , and the Global Positioning System [Cox, 1978] is an area where much investigation is going on and should be continued to obtain the best possible positioning tool. The major advantage that the inertial system has over the systems described above is that the unit is totally self-contained with no external effects such as the refraction of electromagnetic waves in the atmosphere to contend with. The major disadvantage is the complexity of the mechanics which must be fully quantified. It may be that the combination of inertial with another positioning device will result in the best positioning tool for certain surveying and navigation problems.

- (ix) With the advent of better and better inertial components the possibility of a Space Stabilized or Rotating Earth system should be further investigated. These systems would require less torquing and perhaps achieve better accuracies by eliminating some of the numerous torques required for the Local Level system.
- (x) Finally there is a great deal of research required to do proper statistical analysis of the Kalman filter results.

To tackle the above recommendations a great deal of cooperation is needed between the disciplines of mechanical, electrical and surveying engineering. Without this cooperation the improvements attained in one discipline may be of a second order magnitude when compared to the current level of development in another discipline.

REFERENCES

- Abramowitz, M. and I.A. Stegun (eds.) (1964). Handbook of Mathematical Functions. Dover reprint, 1965.
- Adams, G.W. (1977). Inertial Survey Data Reduction Using Maximum likelihood Estimation. Proceedings of the 1st International Symposium on Inertial Technology for Surveying and Geodesy. Ottawa, Canada, October.
- Boyce, W.E. and R.C. DiPrima (1965). Elementary Differential Equations and Boundary Value Problems. 2nd ed., Wiley.
- Britting, K.R. (1971). Inertial Navigation Systems Analysis. Wiley - Interscience.
- Cox, D.B. (1978). Integration of GPX with Inertial Navigation Systems. Journal of the Institute of Navigation. Vol. 25, No. 2.
- Faddeev, D.K. and V.N. Faddeeva (1963). Computational Methods of Lineary Algebra. Transl. from Russian by R.C. Williams, Freeman.
- Farrell, J.L. (1976). Integrated Aircraft Navigation. Academic Press.
- Gentry, D.E., J.A. D'Appolito and J.F. Kasper (1975). Alternative Approaches to Integrated Airborne OMEGA/Inertial Navigation. Journal of the Institute of Navigation. Vol. 22, No. 3.
- Greenwood, D.T. (1965). Principles of Dynamics. Prentice-Hall.
- Hadfield, M.J. (1977). Critical Inertial System Characteristics for Land Surveying. Proceedings of the 1st International Symposium on Inertial Technology for Surveying and Geodesy. Ottawa, Canada, October.
- Heiskanen, W.A. and H. Moritz (1967). Physical Geodesy. Freeman
- Huddle, J.R. (1977). The Theoretical Principles for Design of the Inertial Surveyor for Position and Gravity Determinations. Proceedings of the 1st International Symposium on Inertial Technology for Surveying and Geodesy. Ottawa, Canada, October.
- International Association of Geodesy (1967). Geodetic Reference System (1967). Geodetic Reference System 1967. Bureau Central de l'Association International de Geodesie, Paris.
- Kalman, R.E. (1960). A New Approach to Linear Filtering and Prediction Problems. Journal of Basic Engr. - Trans. ASME, March.

- Kayton, M. (1960). Coordinate Frames in Inertial Navigation. Ph.D. thesis, Massachusetts Institute of Technology.
- Krakiwsky, E.J. and D.E. Wells (1971). Coordinate Systems in Geodesy. Department of Surveying Engineering Lecture Note 16, University of New Brunswick, Fredericton, Canada.
- Krakiwsky, E.J. (1975). A Synthesis of Recent Advances in the Method of Least Squares. Department of Surveying Engineering Lecture Note 42, University of New Brunswick, Fredericton, Canada.
- Liebelt, P.B. (1967). An Introduction to Optimal Estimation. Addison-Wesley.
- Macomber, M.M. (1966). The Influence of Anomalous Gravity on the Performance of a Mechanically - Perfect Inertial Navigation System. Ph.D. Thesis, Ohio State University.
- Mueller, I.I. (1969). Spherical and Practical Astronomy as Applied to Geodesy. Ungar.
- Savage, P.G. (1978). Strapdown Sensors. Advisory Group for Aerospace Research and Development Lecture Series No. 95, Strap-Down Inertial Systems. NATO.
- VanBronkhorst, A. (1978). Strapdown System Algorithms. Advisory Group for Aerospace Research and Development Lecture Series No. 95, Strap - Down Inertial Systems. NATO.
- Vanicek, P. and E.J. Krakiwsky (in prep.). The Concepts of Geodesy. North-Holland.
- Wells, D.E. (1971). Matrices. Department of Surveying Engineering Lecture Note 15, University of New Brunswick, Fredericton, Canada.

Appendix I

Nomenclature

Because of the complexity of inertial navigation many symbolic abbreviations have been made throughout this thesis. The purpose of this appendix is to provide the reader with a list of the various symbols along with a brief description or definition. Where possible the notation convention has been kept consistent with the lecture notes from the Surveying Engineering Department at the University of New Brunswick and also with the text of Farrell [1976].

The first symbols presented are those that are used in general applications, namely

- ($\dot{\quad}$) = first derivative with respect to time,
- ($\ddot{\quad}$) = second derivative with respect to time,
- ($\vec{\quad}$) = vector quantity,
- (\quad)^T = transpose,
- (\quad)⁻¹ = inverse,
- ($\hat{\quad}$) = predicted component,
- (\quad)⁰ = initial value.

The second set of symbols represent more specialized quantities, namely

A - design matrix

\vec{a}_{SA} - absolute acceleration along sensor axes

a - semi-major axis of reference ellipsoid

$()_{AT}$ - Average Terrestrial frame
 b - semi-minor axis of reference ellipsoid
 D - covariance matrix
 γ - normal gravity
 $()_{DR}$ - gyro drift component
 e - first eccentricity of ellipsoid
 $()_E$ - Earth frame component
 f - specific force
 G - Kalman gain matrix
 h - ellipsoid height
 I - identity matrix
 $()_I$ - Inertial frame component
 λ - geodetic longitude
 ℓ - combined earth rate and longitude velocity
 L - observed quantity
 $()_{LL}$ - Local Level frame component
 M - meridian radius of curvature
 N - prime vertical radius of curvature
 $()_P$ - polar motion component
 $()_{PL}$ - platform axes component
 P_m - weight matrix of model errors
 $()_{RE}$ - Rotating Earth axes component
 R_n^m - rotation matrix that rotates from coordinate frame m
 into coordinate frame n
 μ - Schuler frequency
 S.D.F. - single degree of freedom
 $()_{SA}$ - sensor axes component

T - Vernal equinox

Φ - Transition matrix

ϕ - geodetic latitude

Ψ - misorientation

\vec{V}_{SA} - absolute velocity along sensor axes

W - misclosure vector

$\vec{\omega}_E$ - angular velocity of Earth frame with respect to Inertial frame

$\vec{\omega}_{LL}$ - angular velocity of Local Level frame with respect to Inertial frame

ω_S - angular velocity of the earth

$\vec{\omega}_{SA}$ - angular velocity of sensor axes frame with respect to Inertial frame

Appendix II

Rotation and Reflection Matrices

The rotation matrices R_1 , R_2 and R_3 each rotate a coordinate system about a certain axis. An R_1 rotation matrix rotates the Y and Z axes about the X axis. An R_2 rotation matrix rotates the X and Z axes about the Y axis. An R_3 rotation rotates the X and Y axes about the Z axis.

The positive direction of rotation for a right handed coordinate system is taken by convention to be counter-clockwise when viewed from the positive end of the axis about which the rotation takes place.

The rotation matrices are given by [Wells, 1971]

$$R_1(\phi) = \begin{bmatrix} 1 & 0 & 0 \\ 0 & \cos \phi & \sin \phi \\ 0 & -\sin \phi & \cos \phi \end{bmatrix}, \quad \text{A-1}$$

$$R_2(\phi) = \begin{bmatrix} \cos \phi & 0 & -\sin \phi \\ 0 & 1 & 0 \\ \sin \phi & 0 & \cos \phi \end{bmatrix}, \quad \text{A-2}$$

$$R_3(\phi) = \begin{bmatrix} \cos \phi & \sin \phi & 0 \\ -\sin \phi & \cos \phi & 0 \\ 0 & 0 & 1 \end{bmatrix}, \quad \text{A-3}$$

in which ϕ is the angle of rotation.

VITA

Candidate's full name: John Richard Callaghan Adams

Place and date of birth: Campbellton, New Brunswick
Canada
January 27, 1955

Permanent address: 120 Dunn's Crossing Road
Apt. 109A
Fredericton, New Brunswick

Schools attended: Three Rivers High School, 1961-1972
Trois Rivières, Quebec

Universities attended: University of New Brunswick,
1972-1977, B.Sc., Engineering
Fredericton, New Brunswick